Machine learning based prediction of biomass pyrolysis with detailed reaction kinetics for thermally-thick particles: from 1D to 0D

Hao Luo[a], Xiaobao Wang[a], Xinyan Liu[a], Lan Yi[a], Xiaoqin Wu[a], Xi Yu[b], Yi Ouyang[c], Weifeng Liu[d], Qingang Xiong[d,]*

[a]*School of Chemistry and Chemical Engineering, Hubei Key Laboratory of Coal Conversion and New Carbon Materials, Wuhan University of Science and Technology, Wuhan, 430081, China*

[b]*Energy & Bioproducts Research Institute (EBRI), Aston University, Aston Triangle, Birmingham, B4 7ET, UK*

[c]*Laboratory for Chemical Technology, Ghent University, Ghent, 9052, Belgium*

[d]*State Key Laboratory of Pulp and Paper Engineering, South China University of Technology, Guangzhou, 510640, China*

**Corresponding author. Email: qingangxiong@scut.edu.cn (Q. Xiong)*

Abstract

In reactor-scale CFD modeling of biomass pyrolysis with thermally-thick particles, zero-dimensional (0D) models coupled with lumped kinetics are commonly used, as they are simple and computationally efficient. However, intra-particle heat transfer, which cannot be directly implemented in 0D models, has significant effects on pyrolysis behaviors of thermally-thick biomass particles. Additionality, lumped kinetics usually fails to predict detailed composition of pyrolysis products. To overcome these issues, a widely-used one-dimensional (1D) model that can directly incorporate intra-particle heat transfer was employed with a detailed pyrolysis kinetics in this work to develop a corrected 0D (Cor-0D) model for accurate CFD modeling of biomass pyrolysis inside thermally-thick particles. Correction coefficients of external heat transfer, particle diameter, and pyrolysis reactions were introduced by comparing predictions of the 1D model with those of the 0D model quantitatively to reflect the effects of respective factors. The comparison demonstrates that if correction coefficients are properly determined, predictions of the developed Cor-0D model are in good agreement with experimental data as well as those of the employed 1D model under various conditions, while the 0D model overestimates mass loss rate and particle heating rate for thermally-thick biomass particles. Considering that correction coefficients are case dependent and determination of their values are tedious, artificial neural network (ANN) was used to correlate correction coefficients as functions of convective heat transfer coefficient, particle size, gas temperature, moisture

content, and particle's dimensionless temperature to derive an ANN-Cor-0D model. Results show that the ANN-Cor-0D model has the same performance as the Cor-0D model.
Keywords: Biomass pyrolysis; Thermally-thick particle; Intra-particle heat transfer; Detailed pyrolysis kinetics; Artificial neural network; Zero-dimensional model

1. Introduction

As an alternative to fossil fuels for reducing greenhouse gas emissions, converting biomass into bioenergy has attracted great attention in recent years [1-4]. Pyrolysis, gasification, and combustion are the main approaches for converting biomass into bioenergy [1, 2]. Among these three approaches, pyrolysis is viewed as one of the most promising technologies as it produces high energy-density bio-oil and biochar from low energy-density raw biomass [5, 6]. Moreover, pyrolysis is the first step of both gasification and combustion, and thus has significant effects on subsequent subprocesses (such as char conversion) [2, 7]. Therefore, increasing understanding of inherent underlined mechanisms of biomass pyrolysis is of paramount importance and prerequisite to develop advanced techniques to harness the horsepower of bioenergy. As biomass pyrolysis is always operated in reactors, revealing intrinsic physicochemical characteristics inside reactors is critical [8].

Due to the complex nature of multiscale transport-reaction coupling [8, 9], revealing intrinsic physicochemical characteristics of reactor-scale biomass pyrolysis poses great challenge to pure experimental techniques. With the rapid advances in computational capability, computational fluid dynamics (CFD) has been increasingly employed in scientific studies and engineering applications of reactor-scale biomass pyrolysis, and viewed as an indispensable complement to experimental investigations [2, 10]. A specific feature of raw biomass is that biomass feedstock is relatively difficult to be crushed to be small particles (less than 0.5 mm) and thermal conductivity of biomass is typically low (e.g., 0.2 W/m/K) [11]. Therefore, Biot number of usually encountered biomass particles is usually far higher than 0.1 (the value to define the so-called thermally-thin regime). For pyrolysis of thermally-thick biomass particles, intra-particle transport processes, especially intra-particle heat transfer, have significant effects on pyrolysis behaviors [12-14]. Thus, to include the effects of intra-particle transport processes, in most cases a one-dimensional (1D) model is typically required in CFD modeling of biomass pyrolysis to consider such effects [3, 15-18].

However, implementing 1D model in reactor-scale CFD modeling of biomass pyrolysis with thermally-thick particles is either complicated or computationally expensive. If the Euler-Euler multi-fluid model (MFM)[19-21] is used, as solid phases are treated as continua,

establishing 1D intra-particle transport equations in the Eulerian diffusion-convection formulation of solid conservation equations is, even if impossible, rather complicated. On the other hand, though implementing 1D intra-particle transport equations in the Euler-Lagrange CFD-DEM model [22, 23] is straightforward, each individual biomass particle needs to be discretized with a large number of grid points (e.g., 50) to obtain accurate intra-particle information (such as local distributions of temperature and pyrolysis rate) [14, 24-27]. Lu et al.[17] found that computational efficiency using a zero-dimensional (0D) model without explicit solving intra-particle processes is more than one order of magnitude faster than that using a 1D model. Papadikis et al. [25, 26] also found that computational cost significantly increases when a 1D model is used. Thus, 0D models are still highly favored in reactor-scale CFD modeling of biomass pyrolysis with thermally-thick particles [1].

Compared with CFD-DEM, MFM is more feasible for CFD modeling of reactor-scale biomass pyrolysis, especially for reactors with large dimensions. Thus, it is urgent to improve 0D models for use in MFM to guarantee both modeling speed and accuracy. So far, a few studies have attempted to improve modeling accuracy of 0D models for future use in MFM. Dong et al.[28] proposed an indirect method to modify reaction-rate constants to account for the influence of intra-particle heat transfer. Zhong et al. [29] adopted a similar method to investigate the effects of intra-particle heat conduction. Joakim et al. [30] attempted to modify a 0D model with kinetic parameters derived from a 1D model. This idea was also adopted by Anna et al. [31], while an interface-based model other than a 1D model was used [32]. Their results show that performance of 0D models is improved by the above-mentioned modifications. However, it can be found that those studies neglect a very important aspect, i.e., the effects of intra-particle transport processes on external transport processes, which for example results in predicting faster but lower pyrolysis rate than actual values at beginning and end of biomass pyrolysis respectively because external heat transfer is overestimated [30]. Our previous study also revealed that intra-particle heat transfer has significant effects on external heat transfer [33]. To this end, a heat transfer corrected isothermal model was proposed in our previous work [24] as a preliminary attempt to account for the effects of intra-particle transport processes on both external transport processes and reaction behaviors. In this work, external heat transfer, drying rate, and pyrolysis rate were all corrected by correction coefficients as binary functions of convective heat transfer coefficient and dimensionless particle temperature $(T_p - T_{p0})/(T_e - T_{p0})$ (T_p is particle temperature, T_{p0} is initial particle temperature, and T_e is equilibrium temperature). The corrected isothermal model shows comparable prediction accuracy as that of the referred 1D model for both thermally-thin and thermally-thick particles,

but with much faster modeling speed. Thus, this effort opens up the gate to establish a paradigm to derive efficient and accurate 0D models from 1D models for reliable MFM of reactor-scale biomass pyrolysis. However, as only two parameters (i.e., convective heat transfer coefficient and dimensionless particle temperature) were considered in this work [24], applicability of the derived corrected isothermal model is rather limited because typically encountered variations of particle's physicochemical properties and operating conditions such as particle diameter and moisture content cannot be included.

It is also worth noting that corrected coefficients proposed in our previous work [24] are case dependent with prescribed operating parameters (such as gas/wall temperature, particle size, and moisture content). But if full-range applicable corrected coefficients covering desired value ranges for different operating parameters are directly determined by calculations from 1D models, computational overhead is huge and may even become unaffordable. With the rapid development of artificial intelligence, machine learning (ML) has shown great potential to significantly reduce computational efforts to determine full-range applicable surrogate models [34-36]. Using particle-resolved direct numerical simulation to solve intra-particle transport processes, Lu et al. [34] used ML to correlate corrected coefficient of heat transfer as a function of particle's physicochemical properties and surrounding conditions, where much computational time was saved. This undoubtedly proves that ML should be also applicable to derive efficient and accurate 0D models from 1D models for reliable MFM of reactor-scale biomass pyrolysis.

In this study, the method proposed in our previous work [24] was first extended to include particle's typical physicochemical properties and operating conditions to derive a more appliable corrected 0D (Cor-0D) model. Then, the 0D, Cor-0D, and 1D models were comprehensively evaluated by experimental data from literature, including both dry and wet biomass feedstocks under various physicochemical and operating conditions. Finally, ML was applied to correlate derived correction coefficients as functions of particle's physicochemical properties and operating conditions, which can be used in MFM as well as CFD-DEM of reactor-scale biomass pyrolysis. It should be noted that in our previous work [24], a lumped simple pyrolysis kinetics was adopted. However, lumped simple pyrolysis kinetics is not able to give information of compositions of gaseous, liquid, and solid products, which are usually highly necessary in practical applications. Thus, a detailed and validated pyrolysis kinetics based on the sum of macro-components (i.e., cellulose, hemicellulose, lignin) [3, 5, 17, 27, 34, 37] was used in this study.

2. The employed detailed pyrolysis kinetics

The detailed kinetic scheme proposed by Debiagi et al. [37], as shown in Fig. 1, was employed to describe pyrolysis reactions in this work. In this kinetics, biomass is modeled by compositions of cellulose (CELL), hemicellulose (hardwood (XYHW), softwood (GMSW), grass (XYGR), lignin (hydrogen-rich lignin (LIGH), oxygen-rich lignin (LIGO), and carbon-rich lignin (LIGC)), and hydrophobic (TGL) and hydrophilic (TANN) extractive components. In addition, carbonaceous residue defined as char and "metaplastic" phase ($G\{X\}_s$) where volatiles are trapped inside the biochar is included. In this kinetics, 32 reactions and 58 species are involved, and elemental analysis can be used to determine compositions of macro-components when experimental data are not available. The source code to determine compositions of macro-components is available on GitHub along with an online tool [38]. Detailed information on this detailed kinetics can be found in Table S1 in the Supplementary Materials.

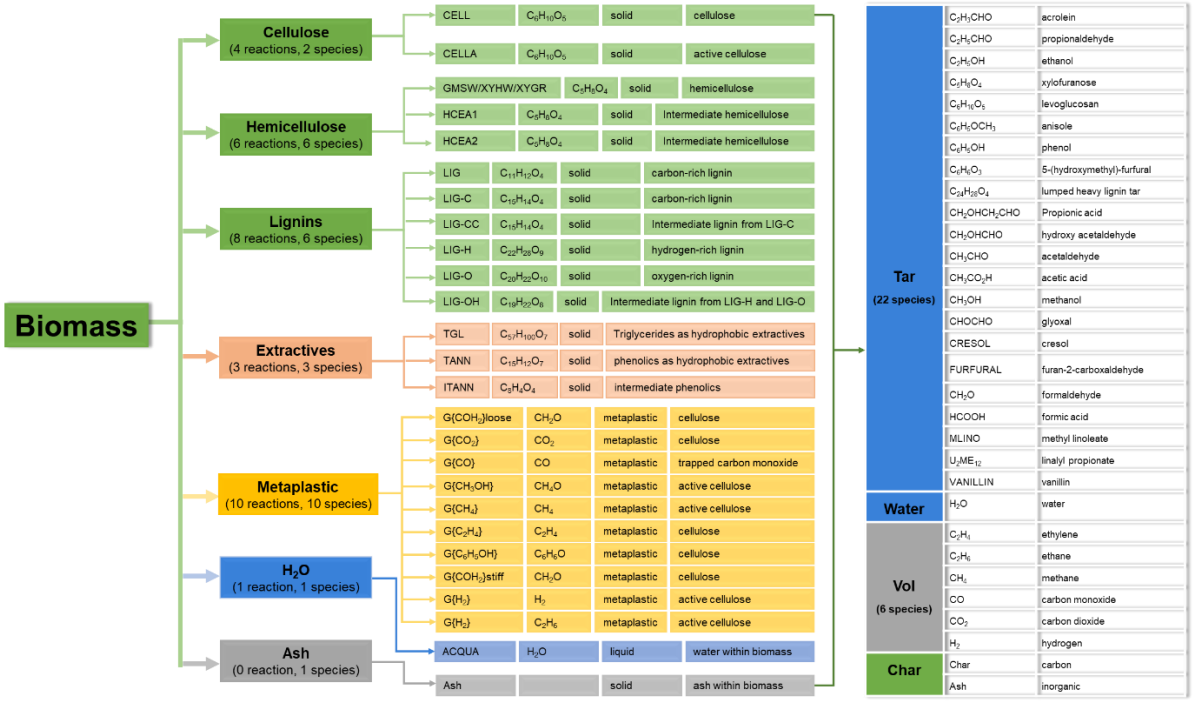

Fig. 1. An illustration of the detailed pyrolysis kinetics reported by Debiagi et al.[37]. Except for moisture and ash, physical properties of other solid species were assumed to be the same as those of raw biomass.

3. Reducing 1D model to 0D model

3.1. The role of intra-particle heat transfer on external heat transfer

To better demonstrate the purpose of deriving Cor-0D models, the role of intra-particle heat transfer on external heat transfer of thermally-thick biomass particles is first discussed. Figure 2 shows the difference in external heat transfer determined by a 0D and 1D model. In all 0D models, uniform temperature distribution inside biomass particles is assumed, while 1D models resolve temperature gradient inside biomass particles considering intra-particle heat transfer. Therefore, the difference between 0D and 1D models can be used to explain the effects of intra-particle heat transfer on pyrolysis behaviors for a thermally-thick biomass particle. The driving force of external heat transfer is temperature difference between particle surface and gas/wall. Considering a thermally-thick particle with the same volume-averaged temperature $T_{p,\mathrm{ave}}$ predicted by 0D and 1D models, particle's surface temperature T_s is equal to both $T_{p,0\mathrm{D}}$ and $T_{p,\mathrm{ave}}$ in 0D models. However, there is temperature gradient inside thermally-thick biomass particles, as demonstrated by 1D models. When heating by external environment, T_s is larger than $T_{p,\mathrm{ave}}$ and $T_{p,1\mathrm{D}}$. Therefore, external heat transfer would be overestimated by 0D models. Considering that pyrolysis rate is strongly determined by intra-particle temperature distribution, intra-particle heat transfer is expected to play an important role in pyrolysis for thermally-thick biomass particles.

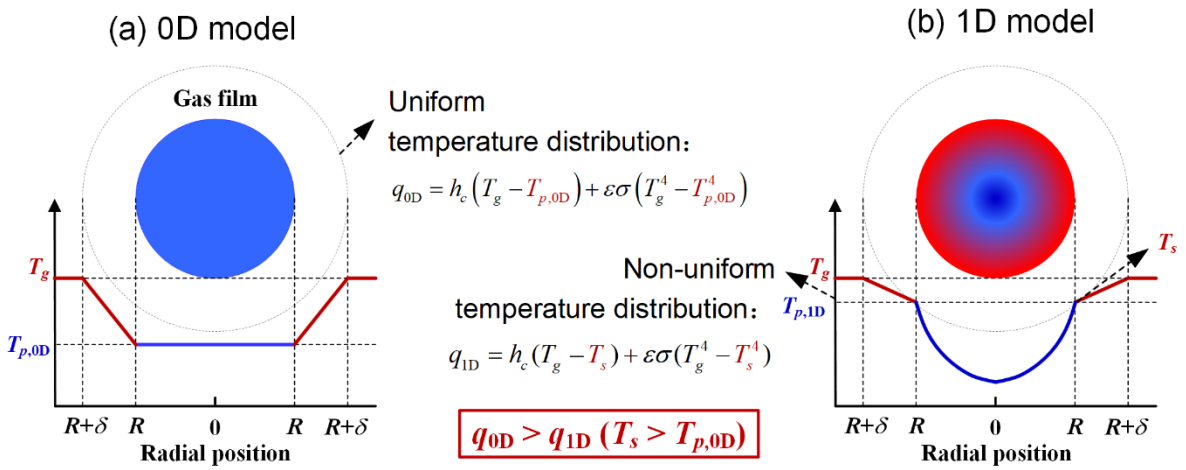

Fig. 2. The effects of intra-particle heat transfer on external heat transfer. $q_{0\mathrm{D}}$ and $q_{1\mathrm{D}}$ are external heat flux predicted by 0D and 1D models, respectively. $T_{p,1\mathrm{D}}$ is intra-particle temperature profile which is solved by 1D models. T_s is particle's surface temperature. Obviously, $T_{p,1\mathrm{D}}$ is not the same as $T_{p,\mathrm{ave}}$ and T_s is larger than $T_{p,\mathrm{ave}}$. To obtain $T_{p,\mathrm{ave}}$ of 1D models, a volume-averaged method should be used. For 0D models, since there is no temperature gradient, $T_{p,0\mathrm{D}}$ is equal to T_s as well as $T_{p,\mathrm{ave}}$.

For 0D models, density $\rho_{i,0D}$ and reaction rate $R_{i,0D}$ of solid species i are uniform throughout the whole particle. However, density $\rho_{i,1D}$ and reaction rate $R_{i,1D}$ of solid species i are remarkably inhomogeneous inside the particle in 1D models. The effects of intra-particle heat transfer on pyrolysis reaction rates can be schematically presented by three stages as shown in Fig. 3. Stage I is the early stage when $T_{p,ave}$ is smaller than $T_{p,crit}$ (named as critical particle temperature when $R_{i,0D}$ is equal to $R_{i,aver,1D}$). At this stage, in 1D models, T_s is relatively high while $T_{p,ave}$ is still relatively low. Therefore, $R_{i,0D}$ is much smaller than $R_{i,ave,1D}$. In Stage II, $R_{i,0D}$ is equal to $R_{i,ave,1D}$. In Stage III, $T_{p,ave}$ is larger than $T_{p,crit}$. At this stage, pyrolysis almost completes as shown in the 1D model, while pyrolysis is still occurring throughout the particle in the 0D model. Thus, $R_{i,0D}$ is larger than $R_{i,ave,1D}$. Overall, intra-particle heat transfer indeed has significant effects on pyrolysis process for thermally-thick biomass particles.

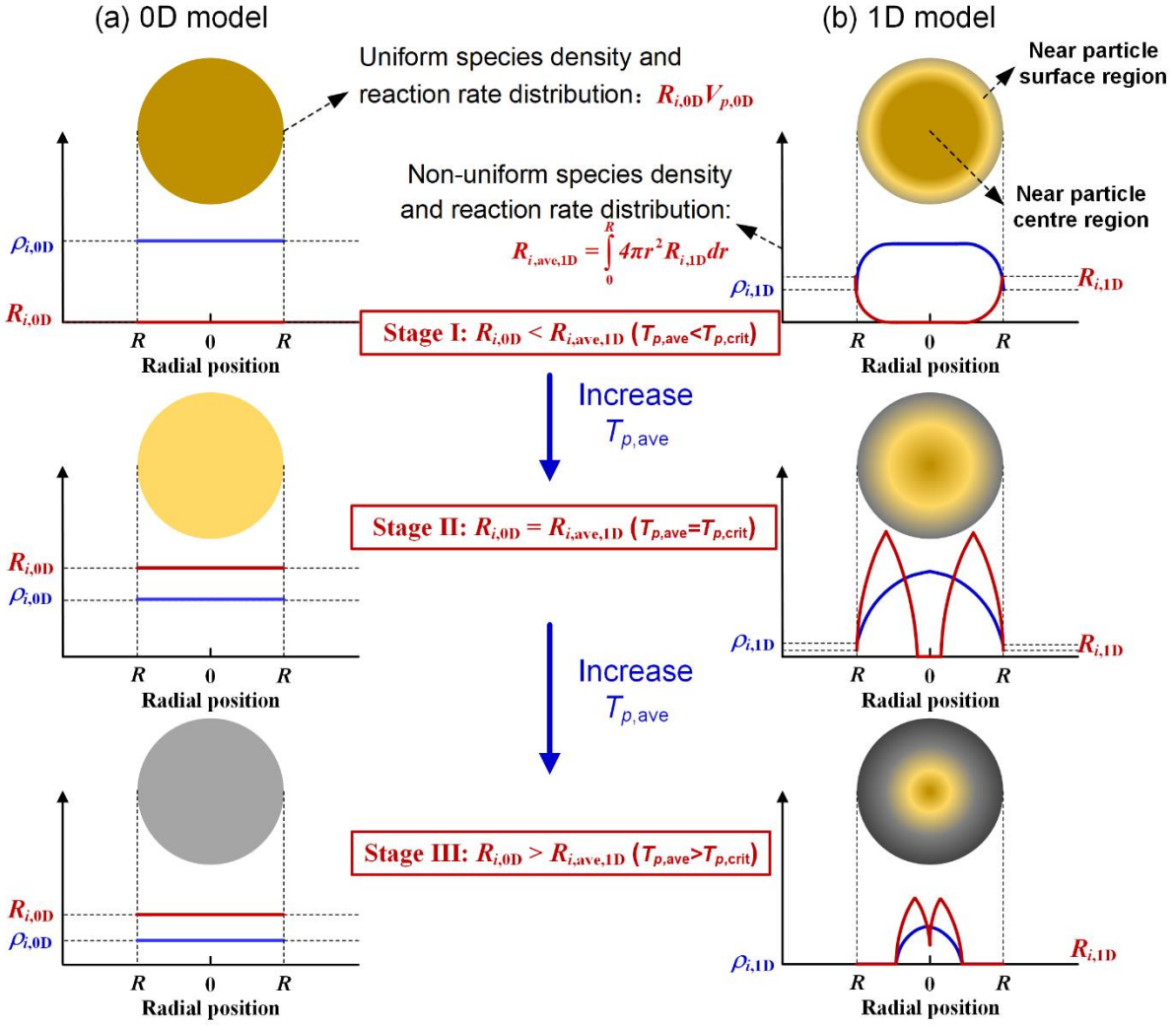

Fig. 3. The effects of intra-particle heat transfer on density and reaction rate of solid species *i*.

3.2. 0D model

The 0D model assumes that temperature is evenly distributed inside the particle. Therefore, the heat balance equation (Eq. (1)), mass balance equation (Eq. (2)), and reaction rate regarding solid species *i* are determined for the whole particle, where external heat transfer flux is given in Eq. (3). Particle shrinkage is described as a function of overall conversion extent as shown in Eq. (4), where the shrinkage coefficient is assumed to be 0.3 which is typical for biomass pyrolysis [5].

$$\begin{aligned}&\left(C_{pB}\rho_{pB,0\mathrm{D}}+C_{pC}\rho_{pC,0\mathrm{D}}+C_{pA}\rho_{pA,0\mathrm{D}}+C_{pW}\rho_{pW,0\mathrm{D}}\right)V_{p,0\mathrm{D}}\frac{dT_{p,0\mathrm{D}}}{dt}\\&=A_{p,0\mathrm{D}}\left(h_c\left(T_g-T_{p,0\mathrm{D}}\right)+\varepsilon\sigma\left(T_w^4-T_{p,0\mathrm{D}}^4\right)\right)+\sum_{j=1}^{32}r_{j,0\mathrm{D}}\Delta H_j V_{p,0\mathrm{D}}\end{aligned} \tag{1}$$

$$\frac{d\left(\rho_{i,0\mathrm{D}}V_{p,0\mathrm{D}}\right)}{dt}=R_{i,0\mathrm{D}}V_{p,0\mathrm{D}} \tag{2}$$

$$q_{0\mathrm{D}}=h_c\left(T_g-T_{p,0\mathrm{D}}\right)+\varepsilon\sigma\left(T_w^4-T_{p,0\mathrm{D}}^4\right) \tag{3}$$

$$d_{p,0\mathrm{D}}=d_{p0}\left(1-\varphi X_{p,0\mathrm{D}}\right) \tag{4}$$

In these equations, C_p (J/(kg·K)) and ρ_p (kg/m^3) are specific heat capacity and particle density, respectively. Subscripts *B*, *C*, *A*, and *W* are raw biomass, char, ash, and moisture, respectively. ΔH_j (J/Kg) is heat of reaction *j*. r_j (kg/(m^3·s) is reaction rate of reaction *j*. $d_{p,0\mathrm{D}}$ (m) is particle diameter, and d_{p0} (m) is initial particle diameter. $V_{p,0\mathrm{D}}$ (m^3) is volume of particle and $A_{p,0\mathrm{D}}$ is particle's external surface aera (m^2), which can be directly calculated by $d_{p,0\mathrm{D}}$. $q_{0\mathrm{D}}$ (W/m^2/s) is external heat flux. *t* (s) is time and h_c (W/m^2/K) is convective heat transfer coefficient. ε and σ are the emissivity (0.85) and Stefan-Boltzmann constant (5.6704×10^{-8} J/(m^2·K^4·s)), respectively. φ is particle shrinkage coefficient (0.3). $X_{p,0\mathrm{D}}$ is extent of particle conversion defined as $(m_0-m_t)/m_0$ where m_0 is initial mass and m_t is mass at time *t*. Pyrolysis reaction rate of reaction *j* is determined by Eq. (5) as

$$R_{j,0\mathrm{D}}=r_{j,0\mathrm{D}}V_{p,0\mathrm{D}} \tag{5}$$

3.3. 1D model

The 1D model that has been used in our previous study [5] was employed in this study. Both intra-particle and external heat transfer are accounted in the model. The heat balance equation is given in Eq. (6) as

$$\frac{\partial\left(C_{pB}\rho_{pB,1D}T_{p,1D}+C_{pC}\rho_{pC,1D}T_{p,1D}+C_{pA}\rho_{pA,1D}T_{p,1D}+C_{pW}\rho_{pW,1D}T_{p,1D}\right)}{\partial t}$$

$$=\frac{1}{r^2}\frac{\partial\left(r^2\lambda_{eff}\dfrac{\partial T_{p,1D}}{\partial r}\right)}{\partial r}+\sum_{j=1}^{32}r_{j,1D}\Delta H_j \tag{6}$$

where λ_{eff} (W/m/K) is effective thermal conductivity. r (m) is radial position within particle. $r_{j,1D}$ (kg/m^3/s) is local reaction rate of reaction j. The mass balance of $\rho_{i,1D}$ in a control volume is given in Eq. (7) as

$$\frac{\partial\left(\rho_{i,1D}\Delta V\right)}{\partial t}=R_{i,1D}\Delta V \tag{7}$$

where ΔV (m^3) is the control volume used in the finite volume method.

Boundary conditions are described in Eq. (8) and Eq. (9) as

$$\left.\frac{\partial T_{p,1D}}{\partial r}\right|_{r=0}=0,\ \text{all}\ \ t \tag{8}$$

$$\left.\lambda_{eff}\frac{\partial T_{p,1D}}{\partial r}\right|_{r=R}=h_c\left(T_g-T_s\right)+\varepsilon\sigma\left(T_w^4-T_s^4\right)\ \ t\geq 0 \tag{9}$$

The initial conditions are

$$T_{p,1D}\left(0,r\right)=T_{p0},\quad \rho_{i,1D}\left(0,r\right)=\rho_{i0},\quad d_{p,1D}\left(0\right)=d_{p0} \tag{10}$$

Heat flux is given in Eq. (11) as

$$q_{1D}=h_c\left(T_g-T_s\right)+\varepsilon\sigma\left(T_w^4-T_s^4\right) \tag{11}$$

Total reaction rate of reaction j is determined by volume integration as

$$R_{j,1D}=\int_0^R 4\pi r^2 r_{j,1D}dr \tag{12}$$

where R (m) is particle radius, which can be determined from $d_{p,1D}$. $T_{p,ave,1D}$ and $\rho_{i,ave,1D}$ are given in Eq. (13) and Eq. (14) as

$$T_{p,ave,1D}=\frac{\int_0^R 4\pi r^2 T_{p,1D}dr}{\int_0^R 4\pi r^2 dr} \tag{13}$$

$$\rho_{i,\mathrm{ave,1D}} = \frac{\int_0^R 4\pi r^2 \rho_{i,\mathrm{1D}} dr}{\int_0^R 4\pi r^2 dr} \tag{14}$$

Particle shrinkage is considered as a sum of each grid as

$$d_{p,\mathrm{1D}} = \sum_{k=1}^{N} \Delta r_k \left(1 - \varphi X_{p,\mathrm{1D}}\right) \tag{15}$$

where N is the number of grid and Δr_k is grid size of the k^{th} grid.

3.4. Corrected 0D model (Cor-0D model)

The main difference between 0D and 1D models is that intra-particle heat transfer is ignored in 0D models but it is accounted in 1D models. Therefore, the effects of intra-particle heat transfer were analyzed by comparing external heat transfer flux and reaction rates determined by the 0D and 1D models. In this work, the method proposed in our previous work [24] was adopted. Assuming the same volume-averaged particle temperature, density of solid species, particle volume for both the 0D and 1D models (namely, $T_{p,\mathrm{ave,1D}} = T_{p,\mathrm{0D}}$, $\rho_{i,\mathrm{ave,1D}} = \rho_{i,\mathrm{0D}}$, and $V_{p,\mathrm{0D}} = V_{p,\mathrm{1D}}$), difference of external heat transfer flux and reaction rates between the 0D and 1D models can be determined as

$$H_T = \frac{q_{\mathrm{1D}}}{q_{\mathrm{0D}}} = \frac{h_c\left(T_g - T_s\right) + \varepsilon\sigma\left(T_w^4 - T_s^4\right)}{h_c\left(T_g - T_{p,\mathrm{0D}}\right) + \varepsilon\sigma\left(T_w^4 - T_{p,\mathrm{0D}}^4\right)} \tag{16}$$

$$H_{R,j} = \frac{R_{j,\mathrm{1D}}}{R_{j,\mathrm{0D}}} = \frac{\int_0^R 4\pi r^2 r_{j,\mathrm{1D}} dr}{r_{j,\mathrm{0D}} V_{p,\mathrm{0D}}} \tag{17}$$

where H_T and $H_{R,j}$ are correction coefficients for external heat transfer flux and reaction rate of reaction j, respectively. Because particle shrinkage of the 0D model is determined by total particle conversion but that of the 1D model depends on local conversion, there will be obvious difference in particle diameter even with the same total particle conversion and volume-averaged particle temperature. Therefore, an extra correction coefficient is defined to describe the effects of intra-particle heat transfer on particle shrinkage as

$$H_D = \frac{d_{p,\mathrm{1D}}}{d_{p,\mathrm{0D}}} = \frac{\sum_{k=1}^{N} \Delta r_k \left(1 - \varphi X_{p,\mathrm{1D}}\right)}{d_{p0}\left(1 - \varphi X_{p,\mathrm{0D}}\right)} \tag{18}$$

Based on the defined correction coefficients, the heat balance equation of the 0D model corrected by H_T is introduced in Eq. (19). In this way, the 1D model is reduced to a 0D model, which is called as corrected 0D model.

$$\begin{aligned}&\left(C_{pB}\rho_{pB,\mathrm{cor}}+C_{pC}\rho_{pC,\mathrm{cor}}+C_{pA}\rho_{pA,\mathrm{cor}}+C_{pW}\rho_{pW,\mathrm{cor}}\right)V_{p,\mathrm{cor}}\frac{dT_{p,\mathrm{cor}}}{dt}\\&=H_T A_{p,\mathrm{cor}}\left(h_c\left(T_g-T_{p,\mathrm{cor}}\right)+\varepsilon\sigma\left(T_w^4-T_{p,\mathrm{cor}}^4\right)\right)+\sum_{j=1}^{32}r_{j,\mathrm{cor}}\Delta H_j V_{p,\mathrm{cor}}\end{aligned}\tag{19}$$

where subscript cor means the corrected 0D model. The mass balance equation has the same formula as Eq. (7), but reaction rate is modified with the correction coefficients for each reaction as

$$r_{j,\mathrm{cor}}=H_{R,j}r_{j,0\mathrm{D}}\tag{20}$$

Particle diameter is also modified with the correction coefficient H_D as

$$d_{p,\mathrm{cor}}=H_D d_{p0}\left(1-\varphi X_{p,\mathrm{cor}}\right)\tag{21}$$

where $d_{p,\mathrm{cor}}$ is particle diameter obtained by the corrected 0D model.

The mass balance equation of the corrected 0D model is given as

$$\frac{d\left(\rho_{i,\mathrm{cor}}V_{p,\mathrm{cor}}\right)}{dt}=R_{\mathrm{i,cor}}V_{p,\mathrm{cor}}\tag{22}$$

According to Eq. (16) as well as our previous studies [24, 33], the correction coefficients can be expressed as binary functions of θ and h_c under predefined conditions (i.e. biomass type, gas and wall temperature), because corresponding particle's surface temperature and solid species density can be determined by Eq. (6) and (7) for a particle with $T_{p,\mathrm{ave,1D}}$. θ is a dimensionless temperature defined as

$$\theta=\frac{T_{p,\mathrm{ave}}-T_{p0}}{T_g-T_{p0}}\tag{23}$$

With given T_{g}, T_w (when radiative heat transfer between wall and particle is included in the model), ρ_{p0}, d_{p0}, T_{p0}, and element analysis of biomass and moisture content, the solution steps to obtain H_T, $H_{R,j}$, and H_D are similar to that of our previous study [24]. In single particle experiments, h_c can be estimated by the Ranz and Marshall equation [39] and it does change much during pyrolysis; therefore, as a fixed convective heat transfer coefficient is usually used in particle-scale modeling, correction coefficients could be reduced as functions of θ. The key steps to derive Cor-0D model are presented below. More details are given in Fig. 4.

Step 1: With given input parameters, solve the 1D model to obtain $T_{p,\mathrm{1D}}$, $\rho_{i,\mathrm{1D}}$, and T_s. Then, $T_{p,\mathrm{ave,1D}}$ and $\rho_{i,\mathrm{ave,1D}}$ are determined by Eq. (13) and Eq. (14). θ is calculated by Eq. (23). q_{1D},

$R_{j,1D}$, and $d_{p,1D}$ are obtained through Eq. (11), Eq. (12), and Eq. (15), respectively. In this way, a series of data (θ, q_{1D}, $R_{j,1D}$, $d_{p,1D}$) are obtained for the given conditions.

Step 2: Assuming that the 0D model has the same volume-averaged particle temperature, average density of solid species i, and particle volume as those of the 1D model, q_{0D}, $d_{p,0D}$, and $R_{j,0D}$ are determined by Eq. (3), Eq. (4), and Eq. (5), respectively. Based on the results, a series of data (θ, q_{0D}, $R_{j,0D}$, $d_{p,0D}$) are obtained.

Step 3: Based on the data from the 0D and 1D models, H_T, $H_{R,j}$, and H_D are determined by Eqs. (16)-(18), respectively. To ensure numerical stability, H_T is specified as 1 when θ is smaller than 0.001 and larger than 0.999, and $H_{R,j}$ is specified as 1 when $R_{j,0D}$ is less than 10^{-6}.

With the obtained correction coefficients, a linear interpolation method was used to fit H_T and $H_{R,j}$, and H_D as functions of θ [40].

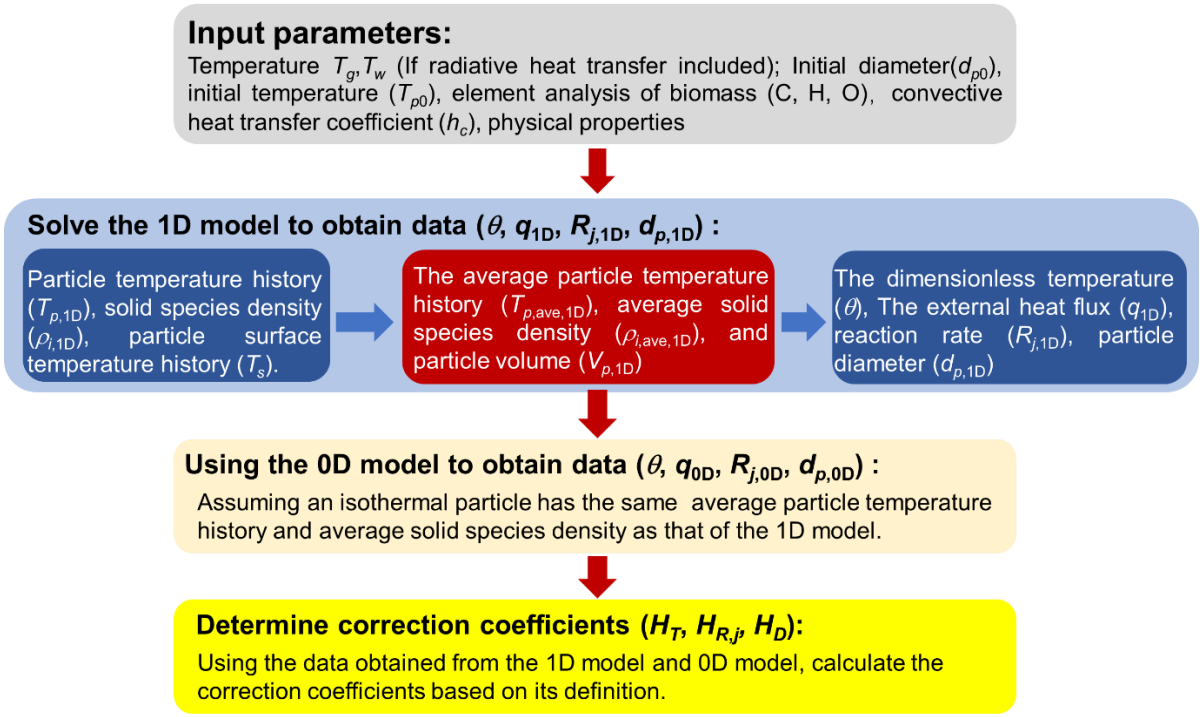

Fig. 4. The solution steps to obtain H_T, $H_{R,j}$, and H_D for the corrected 0D model.

3.5. Physicochemical properties

Table 1 shows the summary of physicochemical properties used in this study. Effective heat conductivity (λ_{eff}) of biomass particle is expressed as a sum of conduction in solid phase (λ_s), gas phase ($\varepsilon_g\lambda_g$), liquid moisture ($\varepsilon_W\lambda_W$), and radiative conduction (λ_r) [30]. Both thermal conductivity of solid phase and particle's pore diameter are assumed to be functions of

pyrolysis degree (η) [15] which is defined as biomass density divided by initial biomass dry density.

Table 1. A summary of physicochemical properties used in this study.

Parameters	Units	Description	Expressions	Ref.
λ_B	W/(m·K)	Dry biomass conductivity	Different values for different wood types	-
λ_C	W/(m·K)	Char conductivity	Different values for different wood types	-
λ_W	W/(m·K)	Water conductivity	$0.278+1.1\times10^{-3}T_p$	[41]
λ_g	W/(m·K)	Gas conductivity	0.0258	[30]
λ_r	W/(m·K)	Radiative conductivity	$\sigma d_{pore} T_p^3/\varepsilon$	[15]
d_{poreB}	m	Wood pore diameter	5.0×10^{-5}	[3]
d_{poreC}	m	Char pore diameter	1.0×10^{-4}	[3]
η	-	Pyrolysis degree	ρ_B/ρ_{B0}	[3]
d_{pore}	m	Average pore size	$\eta d_{poreC}+(1-\eta)d_{poreB}$	[15]
ε_g	-	Particle porosity	$1-\frac{\rho_B+\rho_C+\rho_A+\rho_W}{\rho_{real}}$	-
λ_s	W/(m·K)	Solid conductivity	$\eta\lambda_C+(1-\eta)\lambda_B$	[15]
λ_{eff}	W/(m·K)	Effective conductivity	$\lambda_g\varepsilon_g+\lambda_s+\lambda_W\rho_W/\rho_{real}+\lambda_r$	[30]
C_{pC}	J/(kg·K)	Char heat capacity	$420+2.09T_p+6.85\times10^{-4}T_p^2$	[41]
C_{pB}	J/(kg·K)	Wood heat capacity	$1500+T_p$	[41]
C_{pW}	J/(kg·K)	Water heat capacity	4180	[42]
C_{pA}	J/(kg·K)	Ash heat capacity	$754+0.586(T-273)$	[41]
$\Delta_{vap}H$	J/kg	Heat of vaporization	$1000(3179-2.5T_p)$	[30]
$\Delta_{ds}H$	J/kg	Heat of desorption	$0.4\Delta_{vap}H\left(1-\frac{Y_W}{Y_{fsp}}\right)^2$	[30]
ΔH_{32}	J/kg	Heat of water drying	$\Delta_{vap}H$, ($Y_w>Y_{fsb}$) $\Delta_{vap}H+\Delta_{ds}H$ ($Y_W\leq Y_{fsb}$)	[30]
Y_{fsb}	-	Fiber saturation point	Max($Y_{fsb}=0.598-0.001T_p$, 0.2)	[30]
ε	-	Emissivity	0.85	[15]
σ	J/(m^2·K^4·s)	Stefan-Boltzmann constant	5.6704×10^{-8}	[15]
d_p	m	Particle diameter	$d_{p0}(1-\varphi)$	[5]
φ	-	Particle shrinkage coefficient	0.3	[5]
X_p	-	Particle conversion	$1-\frac{m_t}{m_0}$	-
h_c	W/(m^2·K)	Convective heat transfer coefficient	Ranz and Marshall equation	[39]

Note: d_{p0} is initial particle diameter (m), m_0 is initial particle mass (kg), and m_t is particle mass (kg) at time t. ρ_{B0} is the initial biomass dry density (kg/m^3).

3.6. A short discussion of the correction coefficients

To show the effects of pyrolysis regime on correction coefficients, different d_{p0} (thermally-thin particle (0.1 mm), transition regime (1 mm), and thermally-thick particle (5, 10, 20 mm)) were selected. Initial mass fraction (given in captions of Fig. 5) of macro-components of maple wood with density of 630 kg/m^3 was selected in the study [43]. Figure 5(a) shows the effects of d_{p0} on H_D. For the thermally-thin particle (0.1 mm) which can be regarded as an isothermal particle, H_D is close to 1 at various θ. With the increases in d_{p0}, H_D is larger than 1 in most regions, and the maximum value is up to 1.12 for the thermally-thick particle with d_{p0} = 20 mm, indicating that particle shrinkage predicted by the 0D and 1D models for thermally-thick particles is quite different. Figure 5(b) presents the dependence of H_T on d_{p0} at various θ. When d_{p0} = 0.1 mm, H_T is almost equal to 1, indicating that the 0D model is sufficient to describe pyrolysis of thermally-thin particles. However, H_T decreases with the increases in d_{p0}, and it can be less than 0.2 for the thermally-thick particle with d_{p0} = 20 mm, indicating that external heat transfer predicted by the 0D and 1D models are significantly different for thermally-thick particles. At the start of heating (θ = 0) and end of pyrolysis (θ = 1), both H_D and H_T are equal to 1.0, because there are no gradients of temperature and solid species density inside particle. For 0 < θ < 1, H_T is smaller than 1, which is in good agreement with the theoretical analysis as shown in Fig. 2.

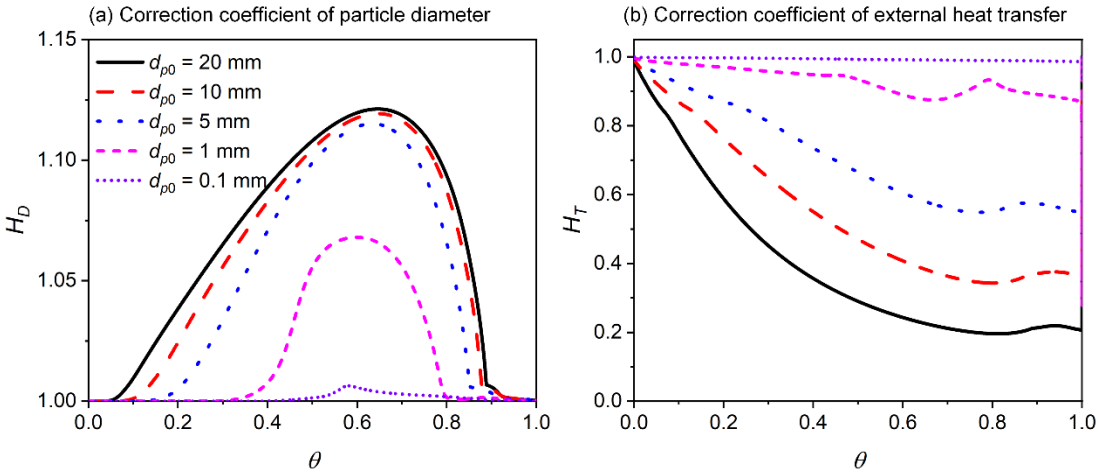

Fig. 5. Correction coefficients of heat flux and particle diameter for particles with different d_{p0} (0.1, 1, 5, 10, 20 mm). (Conditions: T_g = T_w = 1276 K, h_c = 20 W/m^2/K, λ_B = 0.1937 W/m/K, λ_C = 0.1405 W/m/K, ρ_{B0} = 630 kg/m^3, T_{p0} = 303 K; Initial mass fraction of macro-components: X_{CELL} = 0.3829, X_{GMSW} = 0.0000, X_{XYHW} = 0.2080, X_{XYGR} = 0.0000, X_{LIGC} =

0.0511, X_{LIGH} = 0.2553, X_{LIGO} = 0.0872, X_{TGL} = 0.0000, X_{TANN} = 0.0000, X_{ash} = 0.0155, X_w = 0.0000)

Figure 6 shows correction coefficients of some selected reactions for different d_{p0} at various θ. For the thermally-thin particle (0.1 mm), values of correction coefficients are close to 1, indicating that intra-particle heat transfer has insignificant effects on pyrolysis reaction rate. However, for the particles within the thermally-thick regime or the transition regime, reaction rates predicted by the 0D and 1D models are significantly different. For all reactions, $H_{R,j}$ first increases with the increase of θ and is larger than 1. After reaching the peak value, $H_{R,j}$ decreases with the increase of θ. It is worth noting that there are critical values for θ when reaction rate predicted by the 1D model equals to that of the 0D model. With further increase of θ, $H_{R,j}$ increases and finally reaches 1, due to the fact that reactant is almost reacted. The trends of these correction coefficients are in good agreement with the discussions in **Section 3.1**.

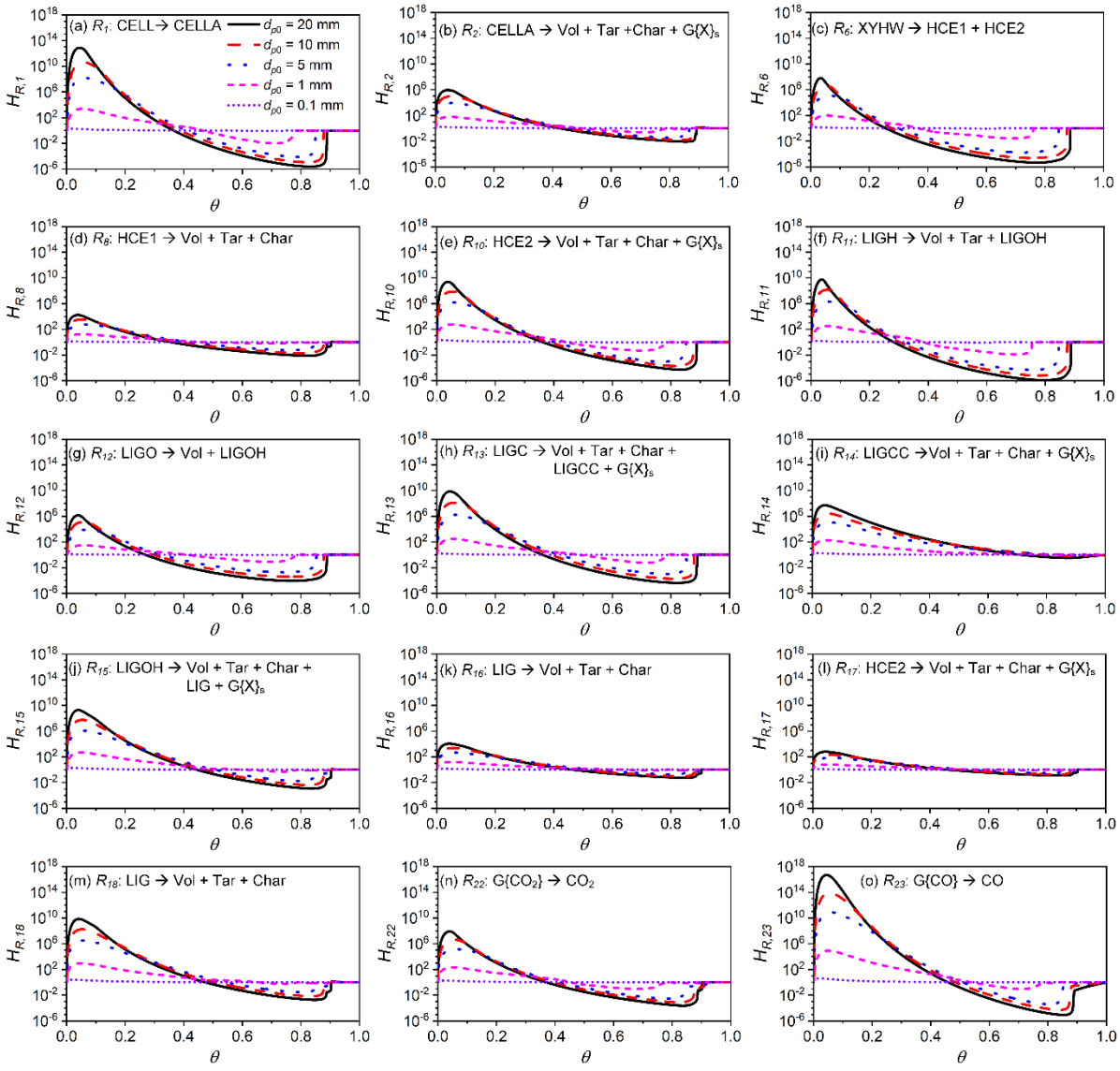

Fig. 6. Correction coefficients of some selected reactions for particles with different d_{p0} (0.1, 1, 5, 10, 20 mm). The input parameters are the same as those in Fig. 5.

Figure 7 shows densities of selected solid species, particle temperature, and particle diameter predicted by the 1D, corrected 0D, and 0D models for the 20 mm particle at 1276 K. For all selected solid species (i.e. CELL, XYHW, LIGH, G{COH_2}$_{Loose}$), density profiles predicted by the corrected 0D model are exactly the same as those of the 1D model, while the 0D model predicts lower reaction (i.e. CELL, XYHW, LIGH)/generation (i.e. G{COH_2}$_{Loose}$, G{COH_2}$_{stiff}$) rates at the beginning and higher ones at the later stage, and peak densities of G{COH_2}$_{Loose}$ and G{COH_2}$_{stiff}$ are much higher than those of the 1D model. Therefore, $H_{R,j}$ larger than 1 at the beginning and less than 1 at the later stage indeed improves performance of the corrected 0D model. For particle temperature, the 0D model gives higher value than that of the 1D model, because of the larger external heat transfer as discussed in Fig.2. The corrected

0D model gives quite a similar particle temperature profile as that of the 1D model. In addition, the particle diameter profiles predicted by the corrected 0D model are almost the same as those of the 1D model.

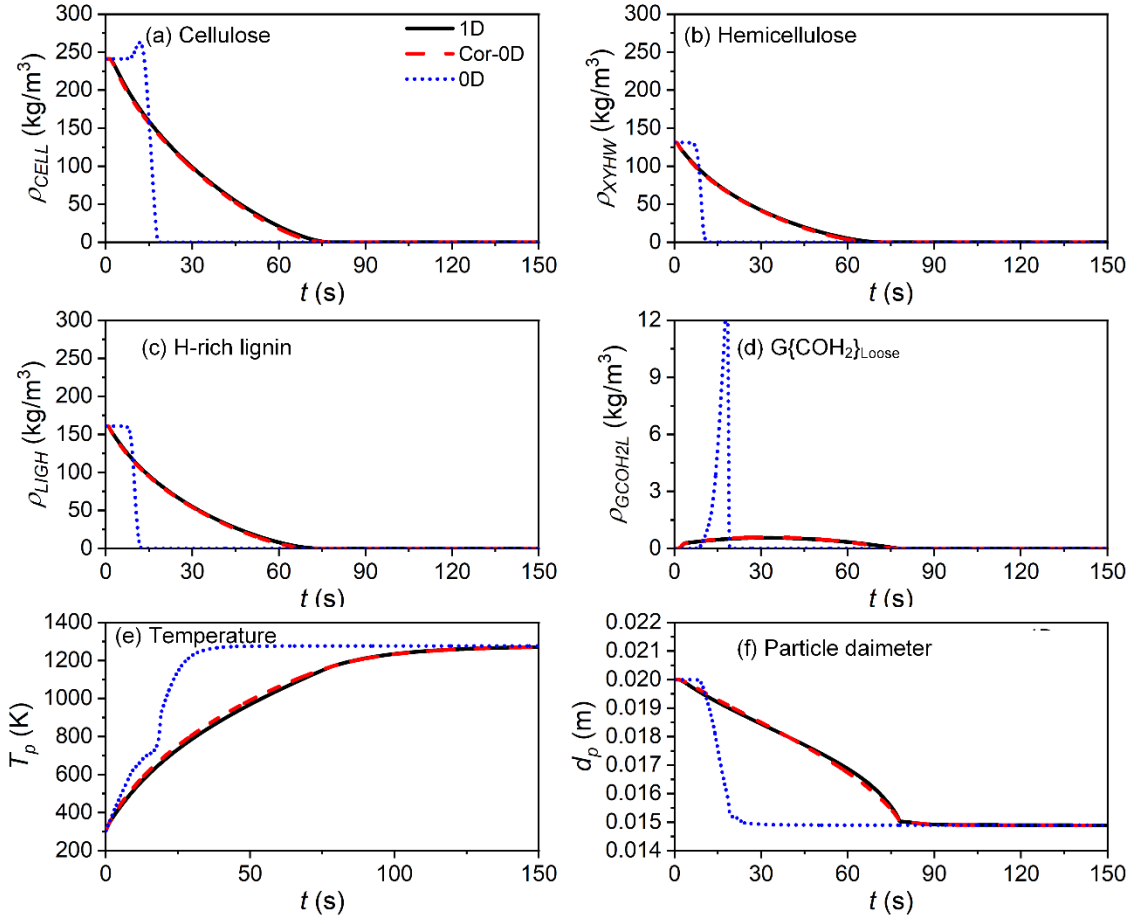

Fig. 7. Densities of selected solid species (a-d), particle average temperature (e), and particle diameter (f) predicted by the 1D, corrected 0D, and 0D models for the 20 mm particle. The input parameters are the same as those in Fig. 5.

4. Model validation

To evaluate performance of the corrected 0D model under various conditions, the experimental data of Park et al. [43] with various T_g, Atreya et al. [44] with various d_{p0} and T_g/T_w, Lu et al. [45] with various moisture content, and Luo et al. [15] with various moisture content, wood type, and T_g were selected for comparison in this study.

4.1. Case 1: Experimental data of Park et al. [43]

In the experiment of Park et al. [43], 24.5 mm maple wood (hardwood) particle was used in a single particle furnace. ρ_{B0} is 630 kg/m^3. T_g was in the range of 585-820 K, and T_w

was slightly higher than furnace temperature. Both particle's center and surface temperature and mass loss history were measured in the experiment. h_c was estimated to be 20 W/m^2/K [43]. Corbetta et al. [46] used a 1D model with a detailed kinetic scheme to model the experiment, and the parameters of physical properties are the same. In our 1D model, particle shrinkage was considered. Details of the experiment of Park et al. [43] are summarized in Table 2.

Table 2. Physicochemical properties and operating conditions of the experiments of Park et al.[43].

Description	Symbol	value
Diameter (mm)	d_{p0}	24.5
Biomass dry density (kg/m^3)	ρ_{B0}	630
Biomass conductivity (W/m/K)	λ_B	0.1937
Char conductivity (W/m/K)	λ_C	0.1405
Macro-components		
Moisture content (dry basis)	X_W	0.0000
Cellulose	X_{CELL}	0.3829
GMSW(Hemicellulose)	X_{GMSW}	0.0000
XYHW(Hemicellulose)	X_{XYHW}	0.2080
XYGR(Hemicellulose)	X_{XYGR}	0.0000
LIGC(Lignins)	X_{LIGC}	0.0511
LIGH(Lignins)	X_{LIGH}	0.2553
LIGO(Lignins)	X_{LIGO}	0.0872
TGL(Extractives)	X_{TGL}	0.0000
TANN(Extractives)	X_{TANN}	0.0000
Ash	X_{ash}	0.0155
Gas temperature (K)	T_g	585/635/670/720/770/820
Wall temperature (K)	T_w	638/688/736/783/831/879
Initial temperature (K)	T_{p0}	303
Convective heat transfer coefficients (W/m^2/K)	h_c	20

Figure 8 shows mass loss measured by Park et al. [43] and predictions using the 0D, Cor-0D, and 1D models. For the 0D model, mass loss rate is overestimated for all temperature conditions, as intra-particle heat transfer is ignored. Moreover, the relative derivation between experiment and model predictions increases with the increases in T_g. The reason is that radiative heat transfer significantly increases with the increases in T_w. For the 1D model, predictions are generally in good agreement with the experimental data, which only slightly underestimates

mass loss rate at low T_g (T_g = 585 K). For the Cor-0D model, predictions are almost the same as those of the 1D model. As compared to the 0D model, accuracy of the Cor-0D model is significantly improved, indicating that the Cor-0D model can well capture the effects of intra-particle heat transfer on pyrolysis reaction rate.

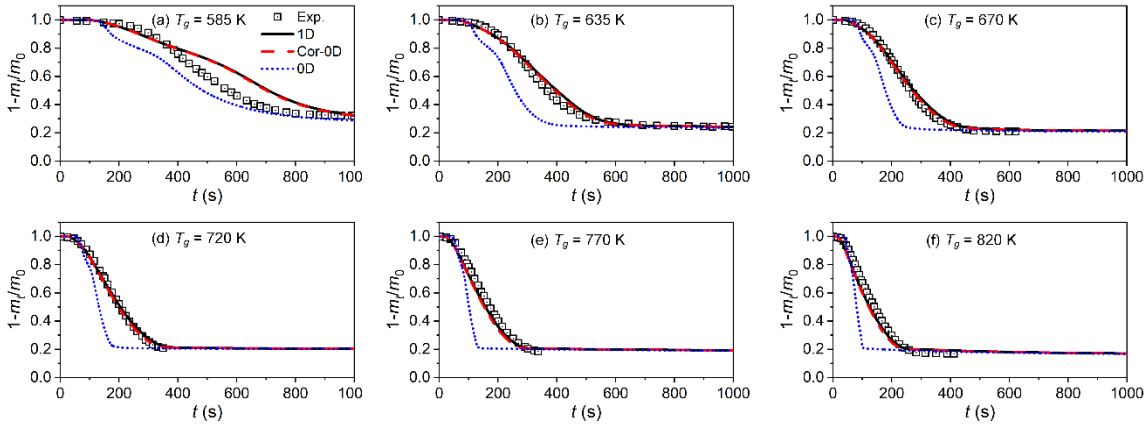

Fig. 8. Comparison of mass loss among Park et al. [43] and different models.

Figure 9 shows the comparison of temperature among Park et al. [43] and different models. For the 0D model, particle heating rate is overestimated, and particle temperature is even larger than the measured particle's surface temperature for the following conditions: T_g = 720 K, 770 K, and 820 K. Since the 0D model overestimates external heat flux, particle temperature predicted by the 0D model is larger than that of the 1D model for all conditions. Considering that pyrolysis kinetics highly depends on particle temperature, the overestimated external heat flux is the main reason for overestimating pyrolysis rate when the 0D model is used. For the 1D model, particle's center and surface temperature are generally in good agreement with the experimental data. The peak value of particle's center temperature at low T_g (i.e., T_g = 635 K, 670 K, and 720 K) caused by exothermic reactions is not correctly predicted by the 1D model, but this has very limited effects on predicting mass loss history. The reason is that the peak of particle's center temperature is not significantly larger (< 50 K) than that of the equilibrium temperature. One may revise enthalpies of pyrolysis reactions as functions of temperature to fit temperature profiles at low temperature conditions [3, 13], instead of using a constant value in this study. For the Cor-0D model, particle temperature profiles predicted by the Cor-0D model are almost the same as those of the 1D model, which is also located between the particle's surface and center temperature, indicating that the Cor-0D model can well capture the effects of intra-particle heat transfer on external heat transfer.

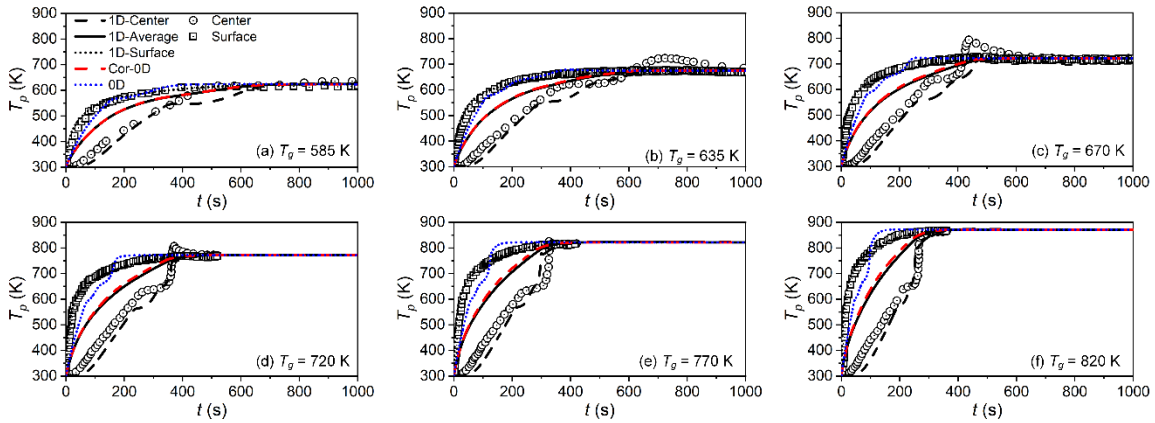

Fig. 9. Comparison of temperature among Park et al.[43] and different models. For the 1D model, both particle's center and surface temperature are available, and volume-averaged temperature of the 1D model is determined by Eq. (13). For the 0D and Cor-0D models, only particle temperature is shown in the figure, as intra-particle heat transfer is not solved.

4.2. Case 2: Experimental data of Atreya et al. [44]

In the experiment of Atreya et al. [44], the wood type (maple wood) is the same as that of Park et al.[43], and three different d_{p0} (10 mm, 15 mm, and 20 mm) were selected. T_g and T_w varied from 743-1133 K and 738-1148 K, respectively. Other parameters of physical properties are the same as those of Case 1. Details of the experiment of Atreya et al. [44] can be found in Table 3.

Table 3. Physicochemical properties and operating conditions of the experiment of Atreya et al. [44].

Description	Symbol	Atreya et al. [44]
Diameter (mm)	d_{p0}	10/15/20
Biomass dry density (kg/m^3)	ρ_{B0}	630
Biomass conductivity (W/m/K)	λ_B	0.1937
Char conductivity (W/m/K)	λ_C	0.1405
Macro-components		
Moisture content (dry basis)	X_W	0.0000
Cellulose	X_{CELL}	0.3829
GMSW(Hemicellulose)	X_{GMSW}	0.0000
XYHW(Hemicellulose)	X_{XYHW}	0.2080
XYGR(Hemicellulose)	X_{XYGR}	0.0000
LIGC(Lignins)	X_{LIGC}	0.0511

LIGH(Lignins)	X_{LIGH}	0.2553
LIGO(Lignins)	X_{LIGO}	0.0872
TGL(Extractives)	X_{TGL}	0.0000
TANN(Extractives)	X_{TANN}	0.0000
Ash	X_{ash}	0.0155
Gas temperature (K)	T_g	743/863/998/1133
Wall temperature (K)	T_w	783/908/1038/1148
Initial temperature (K)	T_{p0}	303
Convective heat transfer coefficients (W/m^2/K)	h_c	20

Figure 10 shows mass loss history measured by Atreya et al. [44] and predictions using the 0D, Cor-0D, and 1D models. At T_g = 743 K, mass loss rate predicted by the 0D model is much faster than that of the experiment, and pyrolysis time is almost 100 seconds shorter than that measured by the experiment for a 20 mm particle. However, mass loss profiles predicted by the 1D model are generally in good agreement with the experimental data. As compared to the 1D model, the Cor-0D model almost gives the same predictions and significantly improves performance of the 0D model. At a higher T_g (e.g., T_g = 1133 K), mass loss rate is underestimated at the beginning stage and then overestimated at the later stage when a 0D model is used. However, predictions of both the 1D and Cor-0D models are similar and agree well with the experimental data. Generally, for all different d_{p0} and T_g, mass loss profiles predicted by the 1D and Cor-0D models are in much better agreement with the experimental data than those of the 0D model.

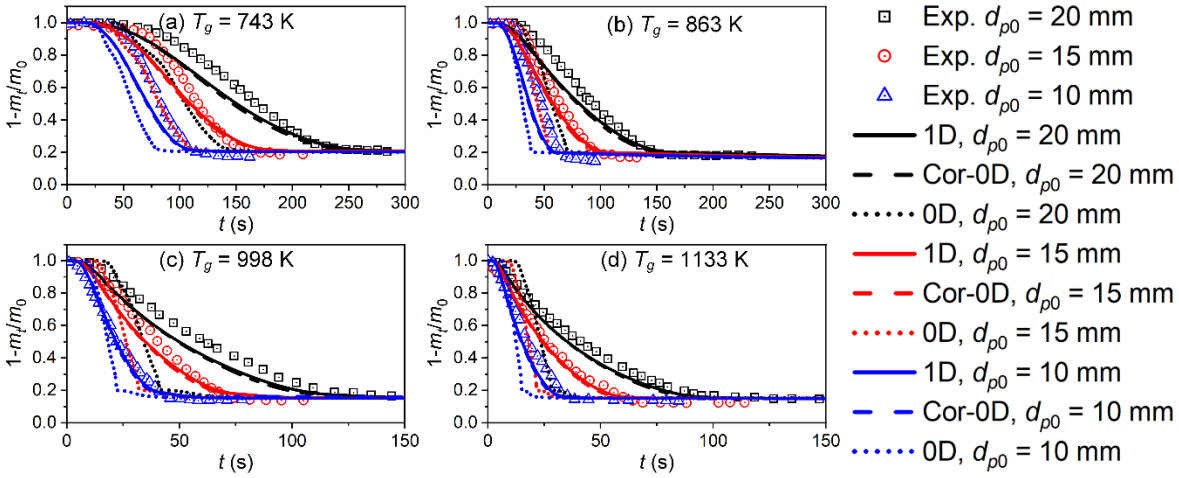

Fig. 10. Comparison of mass loss among Atreya et al. [44] and different models.

4.3. Case 3: Experimental data of Lu et al. [45]

In the experiment of Lu et al. [45], the wood type is polar wood, which is significantly different from maple wood and physicochemical properties (i.e., thermal conductivity of raw biomass and char) are significantly different [47]. Therefore, simulating the case of Lu et al. [45] can also evaluate performance of the Cor-0D model with different feedstocks. T_g and T_w are 1050 and 1276 K, respectively. d_{p0} is 9.5 mm. Moisture content of the polar wood are 6.38% (dry basis) and 66.67% (dry basis), respectively. h_c is estimated by the Ranz and Marshall equation [39], which is approximately 29 W/m^2/K. Details of the experiment of Lu et al. [45] can be found in Table 4.

Table 4. Physicochemical properties and operating conditions of the experiments of Lu et al. [45].

Description	Symbol	Lu et al. [45]
Diameter (mm)	d_{p0}	9.5
Biomass dry density (kg/m^3)	ρ_{B0}	580
Biomass conductivity (W/m/K) [23]	λ_B	3.8(0.1941ρ_{B0}/1000+0.01864)/3.0
Char conductivity (W/m/K) [15]	λ_C	0.071
Macro-components [46]		
Moisture content (dry basis)	X_W	0.0638/0.6667
Cellulose	X_{CELL}	0.4806
GMSW(Hemicellulose)	X_{GMSW}	0.0000
XYHW(Hemicellulose)	X_{XYHW}	0.2611
XYGR(Hemicellulose)	X_{XYGR}	0.0000
LIGC(Lignins)	X_{LIGC}	0.0214
LIGH(Lignins)	X_{LIGH}	0.0957
LIGO(Lignins)	X_{LIGO}	0.1325
TGL(Extractives)	X_{TGL}	0.0000
TANN(Extractives)	X_{TANN}	0.0000
Ash	X_{ash}	0.0086
Gas temperature (K)	T_g	1050
Wall temperature (K)	T_w	1276
Initial temperature (K)	T_{p0}	298
Convective heat transfer coefficients (W/m^2/K)	h_c	29

Figure 11(a) shows the comparison of mass loss history among Lu et al. [45] and different models for a 9.5 mm particle with moisture content of 6.38% (dry basis). Mass loss profiles predicted by the 1D and Cor-0D models are slightly faster than those of the experimental data. However, it is much better than prediction of the 0D model. For particle temperature, as shown in Fig. 11(b), predictions of the Cor-0D model are generally in good agreement with those of the 1D model. However, temperature heating rate predicted by the 0D model is much faster than those of the 1D and Cor-0D models. For the 0D model, time to reach equilibrium temperature is about 15 seconds, which is much faster than that of the experimental data (35 seconds). For the case with high moisture content (66.67%), the 0D model provides a good prediction at the beginning when evaporation of moisture is occurring, as enthalpy of moisture evaporation is rather large and temperature rising rate is rather small, as shown in Fig.11(c) and (d). When drying is completed, mass loss rate is significantly overestimated by the 0D model, while the 1D and Cor-0D models still give reasonable predictions of mass loss profiles, indicating that the Cor-0D model is applicable to describe pyrolysis behaviors of the moisture wood particle.

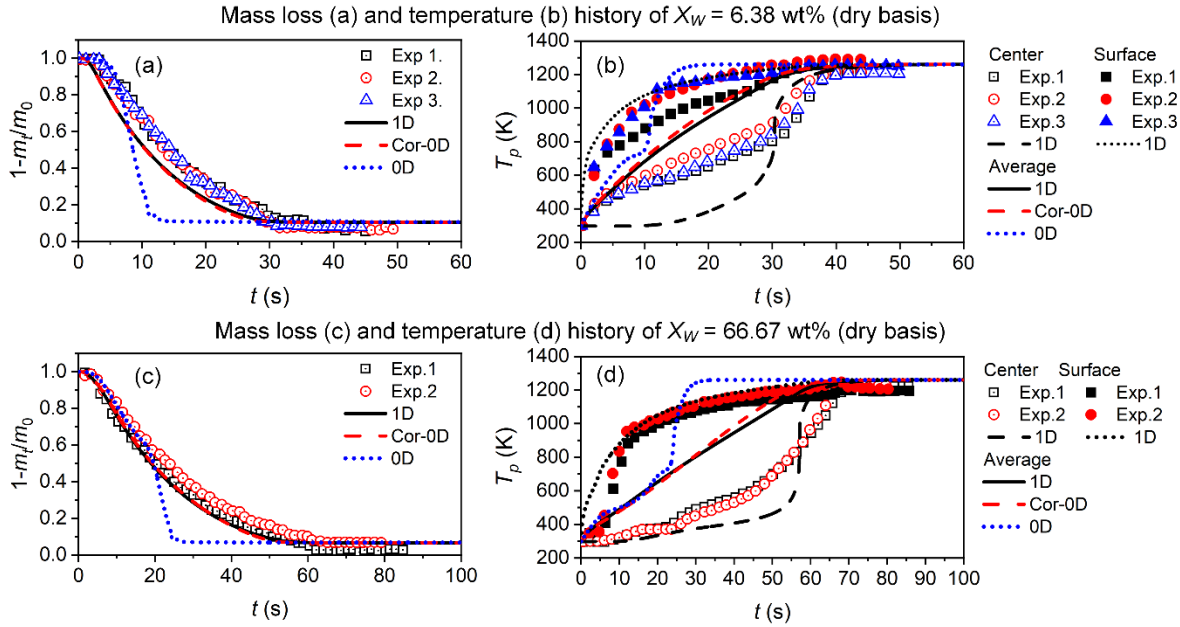

Fig. 11. Comparison of mass loss and temperature among Lu et al. [45] and different models. For the 1D model, both particle's center and surface temperature are available, and volume-averaged temperature of the 1D model is determined by Eq. (13). For the 0D and Cor-0D models, only particle temperature is shown in the figure, as intra-particle heat transfer is not solved.

4.4. Case 4: Experimental data of Luo et al. [15]

To further evaluate whether the Cor-0D model is applicable in pulverized fuel combustion conditions, the experimental data of Luo et al. [15] was selected in this study. In the experiment, a single particle combustor designed for combustion studies of fuel particles with local conditions like those in pulverized fuel fired boilers was used. An individual wood particle is held by a 0.3 mm titanium wire on a ceramic sample probe and suspended in flue gas from hydrogen flame. Three types of wood (i.e., beech, bamboo, and pine) were selected as raw material to evaluate the effects of wood types on pyrolysis process. d_{p0} is around 4 mm. Mass of each wood particle was measured during the experiment and corresponding density was calculated. Range of ρ_{B0} is 400-1200 kg/m^3. To produce wetted wood particles with different moisture content, selected particles were submerged in deionized water. Then they were taken out and exposed to air to obtain a specified moisture content. The range of moisture content is 5%-60% (dry basis). The experiment was carried out in the single particle combustor with different T_g of 1487/1630/1673/1714/1481(wet test) K. h_c is estimated by the Ranz and Marshall equation [39], which is approximately 155 W/m^2/K. Macro-components can be estimated by the method reported by Debiagi et al.[48], as element analysis (C/H/O composition) was measured. Pyrolysis time is a sum of ignition and pyrolysis time, and the method to determine pyrolysis time be found in our previous work [49]. In the modeling, pyrolysis time was determined by particle temperature where 95% of the equilibrium temperature was reached, which is similar to that reported by Remacha et al. [50]. More details on the operating conditions and physical properties can be found in Table 5.

Table 5. Physicochemical properties and operating conditions of the experiments of Luo et al. [15].

Description	Symbol	Luo et al. [15]		
		Beech	Bamboo	Pine
Diameter (mm)	d_{p0}	4		
Biomass dry density (kg/m^3)	ρ_{B0}	400-1200		
Biomass conductivity (W/m/K)	λ_B	3.8(0.1941ρ_{B0}/1000+0.01864)/3.0		
Char conductivity (W/m/K)	λ_C	0.071		
Macro-components				
Moisture content (dry based)	X_W	0.0500-0.6000		
Cellulose	X_{CELL}	0.5007	0.3986	0.4362

GMSW(Hemicellulose)	X_{GMSW}	0.2197	0.0000	0.2370
XYHW(Hemicellulose)	X_{XYHW}	0.0000	0.2767	0.0000
XYGR(Hemicellulose)	X_{XYGR}	0.0000	0.0000	0.0000
LIGC(Lignins)	X_{LIGC}	0.0378	0.0950	0.1034
LIGH(Lignins)	X_{LIGH}	0.0366	0.0046	0.1340
LIGO(Lignins)	X_{LIGO}	0.1422	0.1613	0.0530
TGL(Extractives)	X_{TGL}	0.0204	0.0277	0.0329
TANN(Extractives)	X_{TANN}	0.0366	0.0171	0.0015
Ash	X_{ash}	0.0060	0.0190	0.0020
Gas temperature	T_g	1487/1630/1673/1714/1481(wet test)		
Wall temperature	T_w	1287/1430/1473/1514/1281(wet test)		
Initial temperature	T_{p0}	298		
Convective heat transfer coefficients (W/m^2/K)	h_c	155		

Figure 12 shows the comparison of pyrolysis time among Luo et al. [15] and different models under various conditions. T_g are 1487/1630/1673/1714 K, respectively. Moisture content is 5.15% (dry basis). For the case with different T_g, pyrolysis time predicted by the 1D and Cor-0D models are in good agreement with the experimental data, while the 0D model underestimates pyrolysis time. The modeling results also show that pyrolysis time seems to increase linearly with the increase of ρ_{B0}, which is consistent to our previous study [15]. With the increase of ρ_{B0}, deviation between prediction by the 0D model and the experimental data increases. A similar conclusion can be drawn from the modeling results of pine and bamboo wood, which are given in Fig. S1 and S2 in the Supplementary Materials. These results indicate that the Cor-0D model is applicable to predict biomass pyrolysis at high temperature conditions.

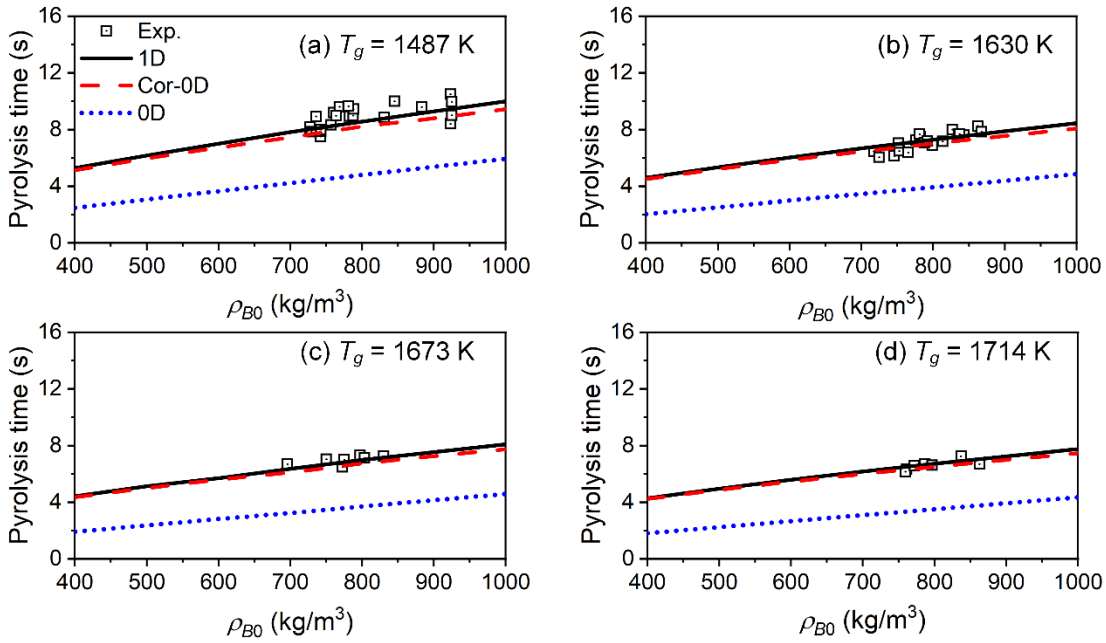

Fig. 12. Comparison of pyrolysis time among Luo et al.[15] and different models under different T_g. The wood type is beech wood. Moisture content is 5.15% (dry basis).

Figure 13 shows the comparison of pyrolysis time among Luo et al.[15] and different models for the beech wood particle with different moisture content. Moisture content varies from 5.15% to 59.83% (dry basis). T_g is 1481 K. As shown in Fig. 13, pyrolysis time predicted by the 1D and Cor-0D models is in good agreement with the experimental data. However, pyrolysis time predicted by the 0D model is much shorter than that of the experimental measurement. Both modeling and experiment show that pyrolysis time increases with the increase of moisture content, because moisture evaporation needs much heat. A similar conclusion can be drawn from the modeling results of pine and bamboo wood with different moisture content, which can be found in Fig. S3 and Fig. S4 in the Supplementary Materials. Considering the Cor-0D model gives a much better prediction than the 0D model for moisture wood, the Cor-0D model is also applicable to predict pyrolysis of wet biomass particles.

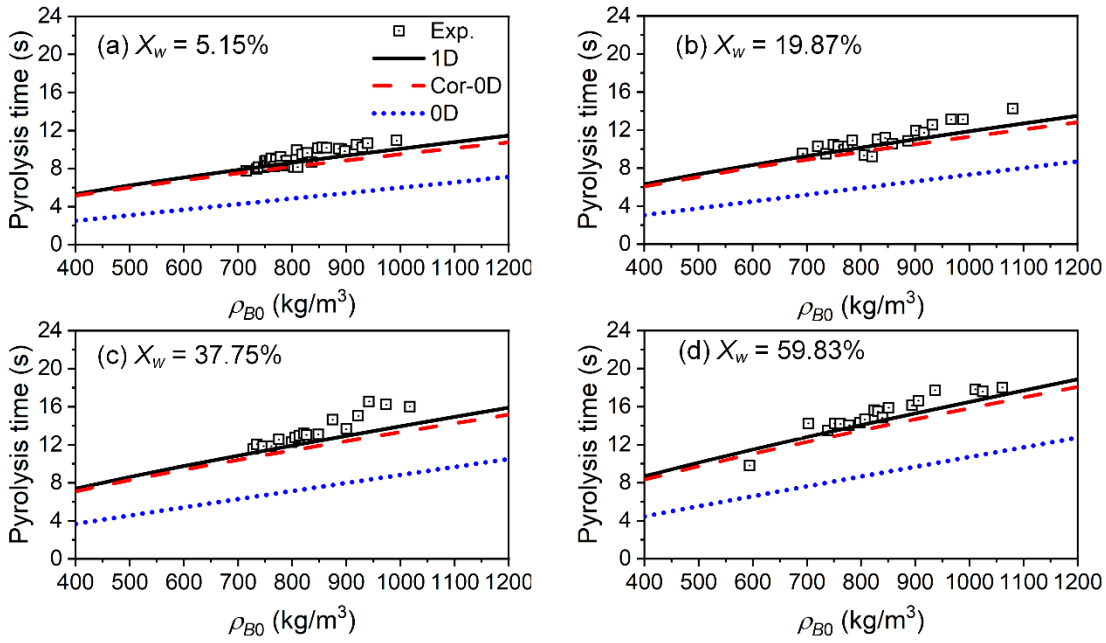

Fig. 13. Comparison of pyrolysis time among Luo et al.[15] and different models for wood particles with different moisture content. The wood type is beech wood. Flue gas temperature is 1481 K.

5. ANN-based corrected 0D model

As shown in Fig. 4, T_g, h_c, d_{p0}, and X_W, etc., are predefined to determine corrected coefficients. Such treatment is a good approximation for single-particle pyrolysis experiments, because particle's surrounding environment does not vary much during pyrolysis. However, surrounding environment of a particle in reactors usually changes obviously, resulting in significantly different h_c and T_g. For example, boundary conditions (e.g., slip velocity, gas composition, gas temperature, solid concentration, etc.) of biomass particles dynamically change in fluidized bed reactors, meaning that h_c also changes dynamically during pyrolysis [24]. Moreover, different feedstocks have different compositions, which has significant effects on pyrolysis and hence correction coefficients. Therefore, to determine correction coefficients for all possible conditions, relevant partial differential equations at each condition are required to be solved as shown in Fig. 4, which is quite time-consuming. In this work, to cover the above-mentioned parameters (i.e., T_g, h_c, d_{p0}, and X_W, etc.) and reduce model complexity to determine correction coefficients, **Step 1** to **Step 3** in **Section 3.4** are first executed for combination of selected parameters (i.e., h_c, d_{p0}, T_g, X_w) to obtain a data matrix of (h_c, d_{p0}, T_g, X_w, θ, $H_{R,j}$, H_T, H_D). Then, the artificial neural network (ANN) was adopted to correlate correction coefficients as functions of (h_c, d_{p0}, T_g, X_w, θ). In this way, the theoretical model is converted to a data-driven surrogate, which is relatively simple and expected to be easily

implemented in CFD. The ANN structure proposed in this work is shown in Fig. 14. The input layer has five parameters (h_c, d_{p0}, T_g, X_w, θ). The output layer is correction coefficients for pyrolysis reactions, external heat transfer, and particle diameter. The number of neurons in the hidden layers was set to 20. The optimization method used in MATLAB is the default method of Levenberg–Marquardt. The activation function used by the hidden layers is the hyperbolic tangent function. The transfer function used by the output layer is a pure linear purlin function, which is an effective model building combination [51]. The database was divided into training (70%), validation (15%), and testing (15%), respectively. The mean squared error (MSE) and squared correlation coefficient were used to evaluate performance of the data-driven surrogate.

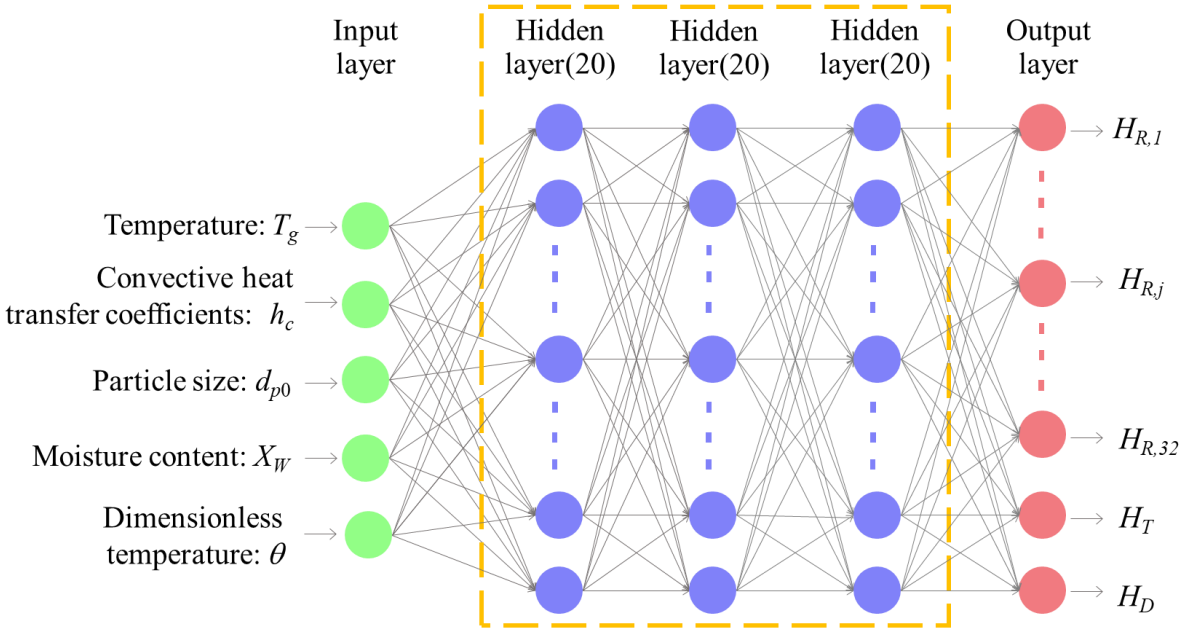

Fig. 14. Structure of the five-layer ANN model for predicting corrected coefficients for the Cor-0D model.

The cases selected to build the ANN model in this work are maple woods which are very typical under biomass pyrolysis, gasification, and combustion conditions. Values of T_g, h_c, d_{p0}, and X_w were randomly selected within the following ranges: 573 K ≤ T_g ≤ 1673 K, 10 W/m^2/K ≤ h_c ≤ 1000 W/m^2/K, 1 mm ≤ d_{p0} ≤ 30 mm, and 0.0 ≤ X_w ≤ 0.5, which covers typical conditions of woody biomass pyrolysis. The total case number is 100. Based on conditions of the selected cases, correction coefficients of each case could be determined as described in Fig. 4, and the number of θ is 1000 for one case. In this way, the database of h_c, d_{p0}, T_g, X_w, θ, $H_{R,j}$, H_T, and H_D was obtained, and matrix size is 39 (5 input parameters plus 34 corrected coefficients)×100×1000. Considering that the range of $H_{R,j}$ may span dozens of magnitudes

(from -8 to 32) as shown in Fig. 5, natural logarithm was applied to $H_{R,j}$ before normalization. Then, the ANN was used to correlate the correction coefficients as functions of h_c, d_{p0}, T_g, X_w, and θ. It is worth noting that that maple wood is hardwood and extractives were not included in the experiment of Park et al. [43]. Hence, the following correction coefficients, i.e., $H_{R,5}$, $H_{R,7}$, $H_{R,19}$, $H_{R,20}$, $H_{R,21}$, and $H_{R,29}$ were not included in the ANN and values of those parameters are 1 in the Cor-0D model. For all correction coefficients, MSE is smaller than 10^{-5} and R^2 is larger than 0.999, indicating good performance of the proposed ANN.

Figure 15 shows the comparison of ANN predictions with the actual values for four typical cases. Input parameters of the four typical cases are listed in Table 6. For particle diameter, correction coefficient predicted by the ANN model is slightly larger than that using the solution steps shown in Fig. 4 for low temperature conditions (Case #1 and #2), but the tendency still matches and the absolute relatively error is smaller than 5%. For Case #3 and #4, correction coefficient predicted by the ANN model is in good agreement with that using the solution steps shown in Fig. 4. For external heat transfer, correction coefficient predicted by the ANN model agrees well with that using the solution steps shown in Fig. 4, where only a slight error is observed when θ is larger than 0.9. For the selected reactions (R_1, R_2, R_6, R_8, R_{10}, R_{11}, R_{12}, R_{13}, R_{14}, R_{15}, R_{16}, R_{17}, R_{18}, R_{22}, R_{23}, and R_{32}), correction coefficients predicted by the ANN model are in relatively good agreement with the actual values from the solutions steps in Fig. 4, although there are differences of about two orders of magnitude. To this end, it can be concluded that the ANN model proposed in this work is a reasonable data-driven surrogate for the solutions steps shown in Fig. 4.

Table 6. Input parameters of the four typical cases used to evaluate the ANN predictions.

Case number	#1	#2	#3	#4
Gas temperature T_g (K)	673	973	1273	1573
Convective heat transfer coefficients h_c (W/m/K)	20	80	200	800
Particle size d_{p0} (mm)	20	15	10	5
Moisture content X_W (dry basis)	0.1	0.3	0.2	0.4

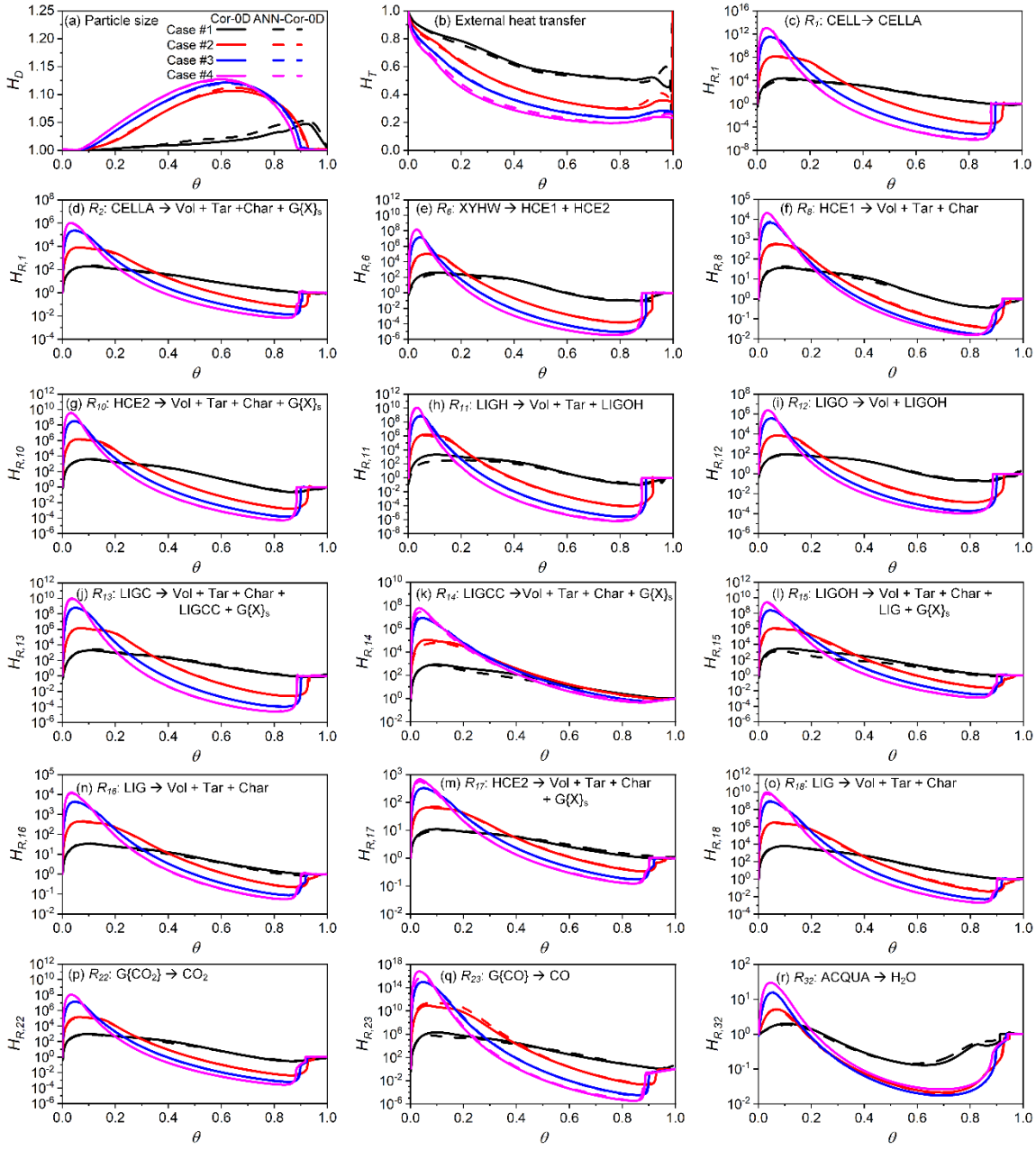

Fig. 15. The comparison of ANN predictions with the actual values for correction coefficients of particle diameter (a), external heat transfer (b), and some selected reactions (R_1, R_2, R_6, R_8, R_{10}, R_{11}, R_{12}, R_{13}, R_{14}, R_{15}, R_{16}, R_{17}, R_{18}, R_{22}, R_{23}, and R_{32}). Conditions of the four selected cases are given in Table 6. The straight line (Cor-0D) is correction coefficient determined through the solution steps shown in Fig. 4. The dashed line (ANN-Cor-0D) is correction coefficient determined from the ANN model shown in Fig. 14.

To further evaluate performance of the ANN model, comparisons of mass loss history and particle temperature predicted by different models are shown in Fig. 16. Input parameters of the selected cases are given in Table 6. For all cases, mass loss rate predicted by the 0D

model is significantly faster than those of the other models, as shown in Fig.15(a), (c), (e), and (g). However, mass loss history predicted by the ANN-Cor-0D model is almost the same as those of the 1D and Cor-0D models. Similar results are observed for particle temperature. Heating rate predicted by the 0D model is significantly faster than those of the other models as shown in Fig. 16(b), (d), (f), and (h), because correction coefficient of external heat flux is smaller than 1. History of particle temperature predicted by the ANN-Cor-0D model is only slightly different from those of the 1D and Cor-0D models. Those results indicate that the ANN model is applicable to predict correction coefficients under various conditions.

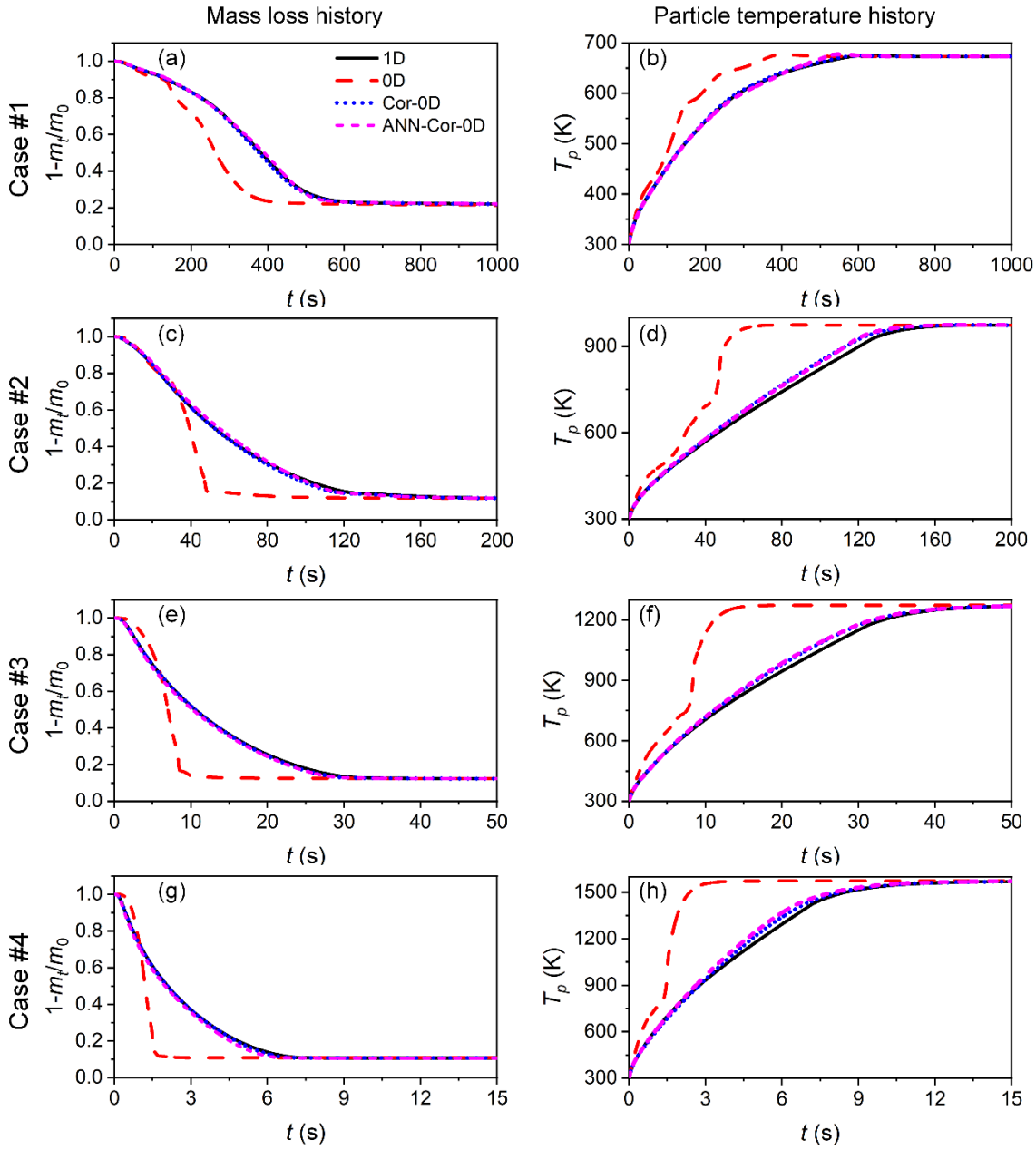

Fig. 16. Comparison of mass loss history and particle temperature among different models for the four typical cases. Input parameters of the four typical cases are given in Table 6.

6. Conclusions and future work

In this work, a corrected 0D model (Cor-0D) coupled with a detailed pyrolysis kinetics was proposed for CFD simulation of pyrolysis of thermally-thick biomass particles. Correction coefficients of external heat transfer, particle diameter, and pyrolysis reactions were introduced by quantitatively comparing predictions of the 1D and 0D models, which aims to capture the effects of intra-particle heat transfer on pyrolysis behaviors. All models were evaluated with four experiments, which cover a wide range of particle size, gas temperature, moisture content, and wood type. The results show that the Cor-0D model shows better performance in predicting all pyrolysis behaviors than the 0D model with almost the same accuracy as the 1D model. Considering that correction coefficients are case dependent and their solutions are time-consuming, the ANN model was adopted to correlate the correction coefficients as functions of convective heat transfer coefficient, particle size, gas temperature, moisture content, and particle's dimensionless temperature to derive an ANN-Cor-0D model. Comparisons show that the ANN-Cor-0D model has the same performance as the Cor-0D model in predicting pyrolysis process for thermally-thick biomass particles. Since the ANN-Cor-0D model does not require solving partial differential equations but with good accuracy, it is expected that the ANN-Cor-0D model will be an efficient and accurate sub-models for future use in reactor-scale CFD modeling of biomass pyrolysis.

Declaration of competing interest

The authors declare that they have no known competing financial interests or personal relationships that could have appeared to influence the work reported in this paper.

Acknowledgment

This study was financially supported by the National Natural Science Foundation of China (No. 22208254 and 22178123), the Scientific Research Foundation of Hubei Educational Committee (No. D20221102), and the Key Laboratory of Hubei Province for Coal Conversion and New Carbon Materials from Wuhan University of Science and Technology (No. WKDM202202 and WKDM202205).

Nomenclature

A_p	Particle surface area	m^2
C_p	Heat capacity of particle	J/(kg·K)
d_p	Diameter of particle	m

h_c	Convective heat transfer coefficient	W/(m^2·K)
H_D	Corrected coefficient for particle diameter	
$H_{R,j}$	Corrected coefficient for reaction *j*	-
H_T	Corrected coefficient for external heat transfer	-
ΔH_j	Heat of reaction *j*	J/kg
m	Mass of particle	kg
q	External heat flux	J/(m^2·s)
r	Radius position	m
r_j	Reaction rate of reaction *j*	kg/m^3/s
R	Radius of biomass particle	m
R_i	Net reaction rate of solid species *i*	kg/m^3/s
R_j	Reaction rate of reaction *j* of the whole particle	kg/s
t	Time	s
T_g	Gas temperature	K
T_s	Particle surface temperature	K
T_p	Particle temperature	K
T_w	Wall temperature	K
V_p	Particle volume	m^3
ΔV	Control volume used in the finite volume method	m^3
X_p	Particle conversion	-

Greek symbols

ε	Emissivity	-
ε_g	Particle porosity	-
φ	Particle shrinkage coefficient	
λ	Conductivity	W/(m·K)
θ	Dimensionless temperature	-
ρ	Density	kg/m^3
σ	Stefan-Boltzmann constant	J/(m^2·K^4·s)

Subscripts

0	Initial conditions
0D	0D model
1D	1D model
A	Ash
ave	Particle volume-averaged
B	Raw biomass

C	Char
cor	Corrected 0D model
crit	Critical particle temperature point when the reaction rate predicted by the 0D model equals to that of the 1D model
g	Gas phase
i	Solid species *i*
j	Reaction *j*
p	Particle
s	Particle surface
t	Value at time *t*
w	Reactor wall
W	Moisture

651

References

[1] H. Luo, X. Wang, X. Liu, X. Wu, X. Shi, Q. Xiong, A review on CFD simulation of biomass pyrolysis in fluidized bed reactors with emphasis on particle-scale models, Journal of Analytical and Applied Pyrolysis 162 (2022) 105433. https://doi.org/10.1016/j.jaap.2022.105433.

[2] Q. Xiong, Y. Yang, F. Xu, Y. Pan, J. Zhang, K. Hong, G. Lorenzini, S. Wang, Overview of Computational Fluid Dynamics Simulation of Reactor-Scale Biomass Pyrolysis, ACS Sustainable Chemistry & Engineering 5(4) (2017) 2783-2798. https://doi.org/10.1021/acssuschemeng.6b02634.

[3] P. Maziarka, A. Anca-Couce, W. Prins, F. Ronsse, A meta-analysis of thermo-physical and chemical aspects in CFD modelling of pyrolysis of a single wood particle in the thermally thick regime, Chemical Engineering Journal 446 (2022) 137088. https://doi.org/10.1016/j.cej.2022.137088.

[4] W. Zhang, X. Qiu, C. Wang, L. Zhong, F. Fu, J. Zhu, Z. Zhang, Y. Qin, D. Yang, C.C. Xu, Lignin derived carbon materials: current status and future trends, Carbon Research 1(1) (2022) 14. https://doi.org/10.1007/s44246-022-00009-1.

[5] H. Luo, X. Wang, K. Krochmalny, L. Niedzwiecki, K. Czajka, H. Pawlak-Kruczek, X. Wu, X. Liu, Q. Xiong, Assessments and analysis of lumped and detailed pyrolysis kinetics for biomass torrefaction with particle-scale modeling, Biomass and Bioenergy 166 (2022) 106619. https://doi.org/10.1016/j.biombioe.2022.106619.

[6] X. Zhang, X. Yang, X. Yuan, S. Tian, X. Wang, H. Zhang, L. Han, Effect of pyrolysis temperature on composition, carbon fraction and abiotic stability of straw biochars: correlation and quantitative analysis, Carbon Research 1(1) (2022) 17. https://doi.org/10.1007/s44246-022-00017-1.

[7] H. Luo, X. Liu, L. Niedzwiecki, X. Wu, W. Lin, B. Lu, W. Wang, H. Wu, Analysis of model dimensionality, particle shrinkage, boundary layer reactions on particle-scale modelling of biomass char conversion under pulverized fuel combustion conditions, Proceedings of the Combustion Institute (2022). https://doi.org/10.1016/j.proci.2022.10.007.

[8] A. Anca-Couce, Reaction mechanisms and multi-scale modelling of lignocellulosic biomass pyrolysis, Progress in Energy and Combustion Science 53 (2016) 41-79. https://doi.org/10.1016/j.pecs.2015.10.002.

[9] M.S. Mettler, D.G. Vlachos, P.J. Dauenhauer, Top ten fundamental challenges of biomass pyrolysis for biofuels, Energy & Environmental Science 5(7) (2012) 7797-7809. https://doi.org/10.1039/c2ee21679e.

[10] F. Alobaid, N. Almohammed, M. Massoudi Farid, J. May, P. Rößger, A. Richter, B. Epple, Progress in CFD Simulations of Fluidized Beds for Chemical and Energy Process Engineering, Progress in Energy and Combustion Science (2021). https://doi.org/10.1016/j.pecs.2021.100930.

[11] M. Masche, M. Puig-Arnavat, P.A. Jensen, J.K. Holm, S. Clausen, J. Ahrenfeldt, U.B. Henriksen, From wood chips to pellets to milled pellets: The mechanical processing pathway of Austrian pine and European beech, Powder Technology 350 (2019) 134-145. https://doi.org/10.1016/j.powtec.2019.03.002.

[12] A. Gómez-Barea, B. Leckner, Modeling of biomass gasification in fluidized bed, Progress in Energy and Combustion Science 36(4) (2010) 444-509. https://doi.org/10.1016/j.pecs.2009.12.002.

[13] H. Ström, H. Thunman, CFD simulations of biofuel bed conversion: A submodel for the drying and devolatilization of thermally thick wood particles, Combustion and Flame 160(2) (2013) 417-431. https://doi.org/10.1016/j.combustflame.2012.10.005.

[14] X. Ku, F. Shen, H. Jin, J. Lin, H. Li, Simulation of Biomass Pyrolysis in a Fluidized Bed Reactor Using Thermally Thick Treatment, Industrial & Engineering Chemistry Research 58(4) (2019) 1720-1731. https://doi.org/10.1021/acs.iecr.8b04778.

[15] H. Luo, Z. Lu, P.A. Jensen, P. Glarborg, W. Lin, K. Dam-Johansen, H. Wu, Experimental and modelling study on the influence of wood type, density, water content, and temperature on wood devolatilization, Fuel 260 (2020) 116410. https://doi.org/10.1016/j.fuel.2019.116410.

[16] H. Fatehi, W. Weng, Z. Li, X.-S. Bai, M. Aldén, Recent Development in Numerical Simulations and Experimental Studies of Biomass Thermochemical Conversion, Energy & Fuels 35(9) (2021) 6940-6963. https://doi.org/10.1021/acs.energyfuels.0c04139.

[17] X. Gao, L. Lu, M. Shahnam, W.A. Rogers, K. Smith, K. Gaston, D. Robichaud, M. Brennan Pecha, M. Crowley, P.N. Ciesielski, P. Debiagi, T. Faravelli, G. Wiggins, C.E.A. Finney, J.E. Parks,

Assessment of a detailed biomass pyrolysis kinetic scheme in multiscale simulations of a single-particle pyrolyzer and a pilot-scale entrained flow pyrolyzer, Chemical Engineering Journal 418 (2021) 129347. https://doi.org/10.1016/j.cej.2021.129347.
[18] L. von Berg, A. Anca-Couce, C. Hochenauer, R. Scharler, Multi-scale modelling of fluidized bed biomass gasification using a 1D particle model coupled to CFD, Fuel 324 (2022) 124677. https://doi.org/10.1016/j.fuel.2022.124677.
[19] H. Zhong, F. Xu, J. Zhang, Y. Zhu, S. Liang, B. Niu, X. Zhang, Variation of Geldart classification in MFM simulation of biomass fast pyrolysis considering the decrease of particle density and diameter, Renewable Energy 135 (2019) 208-217. https://doi.org/10.1016/j.renene.2018.11.097.
[20] Q. Xiong, S.-C. Kong, A. Passalacqua, Development of a generalized numerical framework for simulating biomass fast pyrolysis in fluidized-bed reactors, Chemical Engineering Science 99 (2013) 305-313. https://doi.org/10.1016/j.ces.2013.06.017.
[21] Q. Xiong, S.-C. Kong, Modeling effects of interphase transport coefficients on biomass pyrolysis in fluidized beds, Powder Technology 262 (2014) 96-105. https://doi.org/10.1016/j.powtec.2014.04.062.
[22] T. Chen, X. Ku, J. Lin, H. Jin, Modelling the combustion of thermally thick biomass particles, Powder Technology 353 (2019) 110-124. https://doi.org/10.1016/j.powtec.2019.05.011.
[23] T. Li, H. Thunman, H. Ström, A fast-solving particle model for thermochemical conversion of biomass, Combustion and Flame 213 (2020) 117-131. https://doi.org/10.1016/j.combustflame.2019.11.018.
[24] H. Luo, W. Lin, K. Dam-Johansen, H. Wu, Heat-transfer-corrected isothermal model for devolatilization of thermally thick biomass particles, Energy & Fuels 34(8) (2020) 9620-9631. https://doi.org/doi.org/10.1021/acs.energyfuels.0c01155.
[25] K. Papadikis, A.V. Bridgwater, S. Gu, CFD modelling of the fast pyrolysis of biomass in fluidised bed reactors, Part A: Eulerian computation of momentum transport in bubbling fluidised beds, Chemical Engineering Science 63(16) (2008) 4218-4227. https://doi.org/10.1016/j.ces.2008.05.045.
[26] K. Papadikis, S. Gu, A.V. Bridgwater, CFD modelling of the fast pyrolysis of biomass in fluidised bed reactors. Part B, Chemical Engineering Science 64(5) (2009) 1036-1045. https://doi.org/10.1016/j.ces.2008.11.007.
[27] L. Lu, X. Gao, M. Shahnam, W.A. Rogers, Simulations of biomass pyrolysis using glued-sphere CFD-DEM with 3-D intra-particle models, Chemical Engineering Journal 419 (2021) 129564. https://doi.org/10.1016/j.cej.2021.129564.
[28] N.H. Dong, K.H. Luo, Q. Wang, Modeling of biomass pyrolysis in a bubbling fluidized bed reactor: Impact of intra-particle heat conduction, Fuel Processing Technology 161 (2017) 199-203. https://doi.org/10.1016/j.fuproc.2016.09.015.
[29] H. Zhong, Q. Xiong, Y. Zhu, S. Liang, J. Zhang, B. Niu, X. Zhang, CFD modeling of the effects of particle shrinkage and intra-particle heat conduction on biomass fast pyrolysis, Renewable Energy 141 (2019) 236-245. https://doi.org/10.1016/j.renene.2019.04.006.
[30] J.M. Johansen, P.A. Jensen, P. Glarborg, M. Mancini, R. Weber, R.E. Mitchell, Extension of apparent devolatilization kinetics from thermally thin to thermally thick particles in zero dimensions for woody biomass, Energy 95 (2016) 279-290. https://doi.org/10.1016/j.energy.2015.11.025.
[31] A. Espekvist, T. Li, P. Glarborg, P.A. Jensen, Determination of zero dimensional, apparent devolatilization kinetics for biomass particles at suspension firing conditions, Energies 14(4) (2021) 1018. https://doi.org/doi.org/10.3390/en14041018.
[32] A. Leth-Espensen, T. Li, P. Glarborg, T. Løvås, P.A. Jensen, The influence of size and morphology on devolatilization of biomass particles, Fuel 264 (2020) 116755. https://doi.org/10.1016/j.fuel.2019.116755.
[33] H. Luo, X. Wang, X. Wu, L. Niedzwiecki, H. Pawlak-Kruczek, X. Liu, Q. Xiong, Multi-fluid modeling of heat transfer in bubbling fluidized bed with thermally-thick particles featuring intra-particle temperature inhomogeneity, Chemical Engineering Journal 460 (2023) 141813. https://doi.org/10.1016/j.cej.2023.141813.
[34] L. Lu, M. Brennan Pecha, G.M. Wiggins, Y. Xu, X. Gao, B. Hughes, M. Shahnam, W.A. Rogers, D. Carpenter, J.E. Parks, Multiscale CFD simulation of biomass fast pyrolysis with a machine learning derived intra-particle model and detailed pyrolysis kinetics, Chemical Engineering Journal 431 (2022) 133853. https://doi.org/10.1016/j.cej.2021.133853.

[35] S. Sharma, S. Dhal, T. Rout, B.S. Acharya, Drones and machine learning for estimating forest carbon storage, Carbon Research 1(1) (2022) 21. https://doi.org/10.1007/s44246-022-00021-5.
[36] H. Zhong, Z. Wei, Y. Man, S. Pan, J. Zhang, B. Niu, X. Yu, Y. Ouyang, Q. Xiong, Prediction of instantaneous yield of bio-oil in fluidized biomass pyrolysis using long short-term memory network based on computational fluid dynamics data, Journal of Cleaner Production 391 (2023) 136192. https://doi.org/10.1016/j.jclepro.2023.136192.
[37] P. Debiagi, G. Gentile, A. Cuoci, A. Frassoldati, E. Ranzi, T. Faravelli, A predictive model of biochar formation and characterization, Journal of Analytical and Applied Pyrolysis 134 (2018) 326-335. https://doi.org/10.1016/j.jaap.2018.06.022.
[38] G. Wiggins, BioComp: A web tool for estimating biomass composition. https://github.com/wigging/biocomp. (Accessed April 01 2023).
[39] W.E. Ranz, W.R. Marshall, Evaporation from drops – Part 1, Chemical Engineering Progress 48 (1952) 141-148.
[40] W. Press, S. Teukolsky, W. Vetterling, B. Flannery, Numerical recipes in C: the art of scientific computing, 2nd ed., Cambridge University Press1992.
[41] I. Haberle, N.E.L. Haugen, Ø. Skreiberg, Combustion of Thermally Thick Wood Particles: A Study on the Influence of Wood Particle Size on the Combustion Behavior, Energy & Fuels 32(6) (2018) 6847-6862. https://doi.org/10.1021/acs.energyfuels.8b00777.
[42] K.M. Bryden, M.J. Hagge, Modeling the combined impact of moisture and char shrinkage on the pyrolysis of a biomass particle☆, Fuel 82(13) (2003) 1633-1644. https://doi.org/10.1016/s0016-2361(03)00108-x.
[43] W.C. Park, A. Atreya, H.R. Baum, Experimental and theoretical investigation of heat and mass transfer processes during wood pyrolysis, Combustion and Flame 157(3) (2010) 481-494. https://doi.org/10.1016/j.combustflame.2009.10.006.
[44] A. Atreya, P. Olszewski, Y. Chen, H.R. Baum, The effect of size, shape and pyrolysis conditions on the thermal decomposition of wood particles and firebrands, International Journal of Heat and Mass Transfer 107 (2017) 319-328. https://doi.org/10.1016/j.ijheatmasstransfer.2016.11.051.
[45] H. Lu, W. Robert, G. Peirce, B. Ripa, L.L. Baxter, Comprehensive Study of Biomass Particle Combustion, Energy & Fuels 22(4) (2008) 2826-2839. https://doi.org/10.1021/ef800006z.
[46] M. Corbetta, A. Frassoldati, H. Bennadji, K. Smith, M.J. Serapiglia, G. Gauthier, T. Melkior, E. Ranzi, E.M. Fisher, Pyrolysis of Centimeter-Scale Woody Biomass Particles: Kinetic Modeling and Experimental Validation, Energy & Fuels 28(6) (2014) 3884-3898. https://doi.org/doi.org/10.1021/ef500525v.
[47] S.M. Mousavi, H. Fatehi, X.-S. Bai, Multi-region modeling of conversion of a thick biomass particle and the surrounding gas phase reactions, Combustion and Flame 237 (2022) 111725. https://doi.org/10.1016/j.combustflame.2021.111725.
[48] P.E.A. Debiagi, C. Pecchi, G. Gentile, A. Frassoldati, A. Cuoci, T. Faravelli, E. Ranzi, Extractives Extend the Applicability of Multistep Kinetic Scheme of Biomass Pyrolysis, Energy & Fuels 29(10) (2015) 6544-6555. https://doi.org/10.1021/acs.energyfuels.5b01753.
[49] M. Momeni, C. Yin, S.K. Kær, T.B. Hansen, P.A. Jensen, P. Glarborg, Experimental Study on Effects of Particle Shape and Operating Conditions on Combustion Characteristics of Single Biomass Particles, Energy & Fuels 27(1) (2012) 507-514. https://doi.org/10.1021/ef301343q.
[50] M.P. Remacha, S. Jiménez, J. Ballester, Devolatilization of millimeter-sized biomass particles at high temperatures and heating rates. Part 2: Modeling and validation for thermally-thin and -thick regimes, Fuel 234 (2018) 707-722. https://doi.org/10.1016/j.fuel.2018.07.017.
[51] X. Liu, J. Wu, Y. Lei, X. Wu, Y. Man, H. Luo, Q. Xiong, Data-driven surrogate optimized and intensified extractive distillation process for clean separation of isopropanol from water: A sustainable alternative, Journal of Cleaner Production 383 (2022) 135475. https://doi.org/10.1016/j.jclepro.2022.135475.